International Journal of Heat and Mass Transfer 218 (2024) 124772

Contents lists available at ScienceDirect

International Journal of Heat and Mass Transfer

journal homepage: www.elsevier.com/locate/ijhmt

Identification of aerothermal heating for thermal protection systems taking into account the thermal resistance between layers

Rafał Brociek [a,*], Edyta Hetmaniok [a], Christian Napoli [b], Giacomo Capizzi [c], Damian Słota [a]

[a] Department of Mathematics Applications and Methods for Artificial Intelligence, Silesian University of Technology, Kaszubska 23, Gliwice, 44-100, Poland
[b] Department of Computer, Control, and Management Engineering, Sapienza University of Rome, Via Ariosto 25, Rome, RM, 00185, Italy
[c] Department of Electrical, Electronics and Informatics Engineering, University of Catania, Viale Andrea Doria 6, Catania, 95125, Italy

ARTICLE INFO

Keywords:
Aerothermal heating
Thermal protection system
Inverse problem
Levenberg-Marquardt method
Thermal resistance

ABSTRACT

In this paper the aerothermal heating of a reusable launch vehicle is reconstructed on the basis of temperature measurements taken in the thermal protection system of this vehicle. The discussed integrated thermal protection system is composed of three layers. Mathematical model, describing the problem, takes into account the dependence on temperature of the material parameters as well as the thermal resistances occurring in the contact zones of the layers, which is a novelty in the proposed approach. For solving the direct problem, the implicit scheme of the finite difference method is applied. Next, by using the solution of the direct problem, the Tikhonov functional is created, which describes the error of the current approximate solution. Whereas for determining the solution of the inverse problem the Levenberg-Marquardt method, modified and adapted to the Tikhonov functional, is used. The paper presents the mathematical model of the problem and the method of solution together with the selected examples illustrating its exactness and stability. In order to better examination of the solution method some various values of parameters are taken in the demonstrated examples.

1. Introduction

Many processes, finding their applications in technics and engineering, must be, very often, at first properly designed, modeled and simulated in order to verify their possible run. Appropriate modeling of the process and execution of the necessary simulations enables to reduce the production costs of the planned product, as well as to minimize the risk and to maximize the safety. In particular such situation takes place in case of processes running in high temperatures. An example of such phenomenon is the spacecraft landing through the atmosphere, where the complicated thermal processes occur, and the vehicle is vulnerable to the serious damages. In that case the thermal protection system (TPS) must be designed with properly selected system geometry and made of the properly chosen materials. To do that the computer modeling is very useful, basing on the, among others, solution of the inverse heat conduction problems (like, for example, the identification of heat flux in outer surface in TPS). It is because the inverse problems enable to select the initial and boundary conditions and the values of coefficients ruling the thermal processes, so that the process runs in strictly determined and required way. Therefore so important is to develop the technics of solution of the inverse problems and the computational algorithms necessary to execute the simulations of running processes.

The review of various thermal protection systems is presented by Uyanna and Najafi in paper [1]. Whereas the review of scientific works concerning the layer constructions for thermal protection systems is presented by Le et al. [2]. Next, Gusarov et al. in paper [3] describe the models of reflection coefficient and heat transfer through the porous material made of carbon fiber, applied in the thermal protection system. Whereas Wang et al. in work [4] present the integrated system of thermal protection which incorporates the graded insulation materials and multi-layer ceramic matrix composite cellular sandwich panels. The thermal and mechanical properties of the proposed system are also examined in this paper.

Direct measurement of the heat flux which heats the reusable launch vehicle entering the atmosphere is very difficult, or even impossible. Therefore so important in practise is a possibility of the heat flux identification on the ground of temperature measurements taken inside of the vehicle. This can be done by using the inverse problems. Some research papers describing the solutions of the inverse problems created

* Corresponding author.
E-mail address: rafal.brociek@polsl.pl (R. Brociek).

https://doi.org/10.1016/j.ijheatmasstransfer.2023.124772
Received 29 May 2023; Received in revised form 30 June 2023; Accepted 28 September 2023
Available online 11 October 2023

Nomenclature

b_s	limits of layers	m
c_s	specific heat in layer s	J/kg K
E	identity matrix	
E_{abs}	absolute error	W/m^2
E_{rel}	relative error	%
F	minimized functional	
h_z	contact conductance for the interface	W/m^2 K
I	number of sought parameters	
J	sensitivity matrix	
k	thermal conductivity	W/m K
m	number of time steps	
n_s	number of nodes in layer s	
N	number of measurements	
p	iteration number	
p_{max}	maximal number of iterations	
q_{at}	aerothermal heat flux	W/m^2
q_{con}	heat flux	W/m^2
q_{est}	estimated heat flux	W/m^2
q_{ex}	exact heat flux	W/m^2
q_{rad}	re-radiation heat flux	W/m^2
r_s	auxiliary parameter in the finite difference method	
R_{12}, R_{23}	thermal resistance	m^2 K/W
S_s	mesh in layer s	
S_t	mesh in time interval	
S_x	spatial mesh in the entire region	
t	time	s
t^*	end of the time interval	s
$\widehat{t}_i$	nodes of interpolation	
T_s	temperature in layer s	K
T_∞	temperature of surrounding	K
U_i	measured temperature	K
V_i	reconstructed temperature in measurement point	K
w_s	auxiliary parameter in the finite difference method	
x	spatial variable	
x_m	location of measurement point	

Greek symbols

γ	regularization parameter	
δ	length of gap	m
Δt	time step	
Δx_s	step mesh in layer s	
ε	surface emissivity	
η_1, η_2	numeric parameters	
μ	damping parameter	
ν	random variable	
ξ	a priori given approximation of the heat flux	
ρ_s	mass density in layer s	kg/m^3
σ	the Stefan-Boltzmann constant $5.67 \cdot 10^{-8}$	W/m^2 K^4
φ	temperature on inner surface	K
ψ_s	temperature in layer s in initial moment	K

for various mathematical models of thermal protection systems are already available.

In particular, Uyanna et al. [5] consider the model composed of three layers which represent an integrated thermal protection system. The model does not assume any conditions in the contact points between the layers and the inverse heat conduction problem, presented in the paper, consists in the identification of an aerothermal surface heat flux of TPS. The problem is solved sequentially in the successive layers, starting from the inner layer. Similar problem is considered in paper [6], but the model presented there is composed only of two layers and for solving the inverse problem the Levenberg-Marquardt method is applied. The same Authors in work [7] investigate the problem of the material selection, their properties and geometric dimensions in the successive layers of TPS. The results, described in this paper, indicate that the best materials in the successive layers should be the silicone impregnated reusable ceramic ablator (SIRCA), Saffil and glass-wool, respectively. Fang et al. [8] solve the direct problem of heat transfer in the multi-layer thermal protection system doped with the phase change materials. Nenarokomov et al. [9] also solve the inverse heat conduction problem consisting in retrieving the heat flux in the thermal protection system of spacecrafts. For this purpose the Authors use the iterated regularization method. Next, Nakamura et al. [10] apply the sequential function specification method and the truncated singular value decomposition in solving the inverse problem for two-dimensional one-layer model. Duda [11] presents an algorithm enabling to reconstruct the heat flux on the outer surface of an atmospheric reentry capsule on the basis of measurements of temperature. Future time steps and smoothing filters are next used to stabilize the solution of an inverse problem. Cui et al. [12] use an inverse problem for estimating the, depending on temperature, thermal conductivity coefficient of an Inconel in the reusable metallic thermal protection system. Alifanov et al. in paper [13] consider the problem of selection of the optimal width of layer, together with the diameter of cell and the porosity of carbon foam, creating one of the layers in the multi-layer thermal shield of the solar probe. Xu et al. in work [14] examine an influence of the distribution of pores in the material, the thermal protection system is made of, on the effectiveness of the whole system. Jiang et al. [15] discuss the multi-layer model with the uncertain thermo-physical parameters, but with no thermal resistances between layers taken into account. The widths of layers are determined with the use of a non-probabilistic optimization process in order to ensure the imposed temperature restrictions. Ren et al. [16] investigate an influence of adding the layer, made of the phase change material, to the thermal protection system on the thermal efficiency of the system. In the considered model the perfect contact (with zero thermal resistances) of the layers is assumed. In paper [17] the Authors solve the inverse problem of the lightweight thermal protection system. By using the sequential function specification method they reconstruct the thermal conditions on the outer surface on the ground of temperature measurements taken inside of the region. The performed simulations, imitating the behavior of lightweight thermal protection system in the blunt body, are described in paper [18]. Finally, Wen et al. in work [19] apply the unscented Kalman filtering technique to reconstruct the surface heat flux and inner temperature field of the thermal protection system, on the basis of temperature measurements.

As mentioned before, in order to successful modeling and simulating the run of thermal processes essential is, very often, to solve the properly formulated inverse problems. In particular, these problems can be useful in case of the need to identify the model parameters. The inverse problems belong to the group of ill-posed problems, that is the problems very sensitive to the noises of input data, in result of which small perturbations of the input data may cause very big differences in the output data. For this reason the inverse problems are very difficult in solving. Therefore the new ideas for solving the inverse problems, related to the specific technical and engineering problems, are constantly required and wanted. In particular one can find in literature the proposals of various computational techniques and modifications of algorithms of different kind dedicated to the solution of inverse heat conduction problems. One of the approaches for solving the inverse problems with the measurement noises is the Tikhonov regularization [20,21], another approach is given by the variational method with an additional numerical regularization parameter, as well as the method of direct iterative regularization. More details and theory in this subject can be found

in [22,23] and [24,25]. Many applications are additionally described in paper [26].

The Levenberg–Marquardt method is a well verified and efficient method for solving many inverse problems. It belongs to the class of iteratively regularized Gauss–Newton methods and one can find in literature its successful applications for solving various ill-posed inverse problems of heat transfer, filtration and geophysics (see for example [27]). Whereas paper [28] presents a modification of the Levenberg-Marquardt method for the Tikhonov operator and proves its convergence under some local conditions. Some other modifications of the Levenberg–Marquardt method are proposed, for example, by Cui et al. in [29] and by Sajedi et al. in [30].

The object of interests of the current paper is the inverse problem consisted in reconstruction of the aerothermal heating conditions for a thermal protection system used in the spacecrafts. An information, necessary for solving the discussed inverse problem, is delivered by the values of temperature measured in the selected point of thermal protection system. The considered integrated thermal protection system of the vehicle [1,5] is composed of three layers. The solution of the corresponding direct problem is obtained by using the implicit scheme of the finite difference method. Basing on the solution of the direct problem, the Tikhonov functional, defining the error of the current approximate solution, is constructed. Whereas for solving the inverse problem the modified Levenberg-Marquardt method [28] is applied. The atmospheric entry heating profile on the surface of the reusable launch vehicle, used in the calculations, was generated at NASA Langley Research Center [31] (see also [6,5]).

In the previous works of the Authors [32,33] one can find an algorithm elaborated for solving the problem for the case of perfect contact between the layers, constant parameters of the material and parameters of the material depending on temperature. Novelty of the model presented in this paper is the thermal resistance between layers taken into account in the model. Parameters of the material, as well as the thermal resistance of substances filling the spaces between layers, depend on temperature. The paper includes the description of mathematical model of the considered system, explanation of the solution method and analysis of the computational examples illustrating the exactness and stability of the proposed approach.

2. Formulation of the problem

The object of interests is a shell composed of three layers. The outer layer is affected by the heat flux, whereas on the surface of inner layer the constant temperature is maintained. Thermal contact between layers is not perfect, that is the thermal resistances occur in substances filling the spaces between layers. Moreover, the coefficients characterizing the materials, the layers are made of, depend on temperature. Distribution of temperature in each layer is described by means of the heat conduction equation [34]:

$$c_s(T)\,\varrho_s(T)\,\frac{\partial T_s(x,t)}{\partial t} = \frac{\partial}{\partial x}\left(k_s(T)\,\frac{\partial T_s(x,t)}{\partial x}\right), \qquad x \in (b_{s-1}, b_s),\ t \in (0,t^*), \tag{1}$$

where c_s, ϱ_s, k_s and T_s, $s = 1,2,3$, denote the specific heat, density, thermal conductivity coefficient and temperature in layer number s, respectively.

Aim of the inverse problem is to reconstruct the aerothermal heat flux (q_{at}) applied on the outer surface. Some part of this heat flux is transferred in the material (q_{con}). Simultaneously, this heat flux causes a heating of the surface that emits a heat flux by radiation (q_{rad}). Thus, the energy balance equation can be written as follows

$$q_{con}(t) = q_{at}(t) - q_{rad}(t). \tag{2}$$

Re-radiation term can be determined basing on the knowledge of temperature

$$q_{rad}(t) = \varepsilon\,\sigma\left(T_1^4(b_0,t) - T_\infty^4\right), \tag{3}$$

where ε means the surface emissivity, σ is the Stefan-Boltzmann constant, and T_∞ denotes the ambient temperature.

Hence, the boundary condition of the second kind, defined on the outer surface, has the form

$$-k_1(T)\,\frac{\partial T_1(x,t)}{\partial x}\bigg|_{x=b_0} = q_{at}(t) - q_{rad}(t), \qquad t \in (0,t^*). \tag{4}$$

Whereas on the inner surface, that is at the end of third layer, the boundary condition of the first kind is given

$$T_3(b_3,t) = \varphi(t), \qquad t \in (0,t^*). \tag{5}$$

Meanwhile, in the spaces of contact of two layers the interface boundary conditions are defined, with the non-zero values of thermal resistances R_{12} and R_{23}. In the contact space between the first and second layers, that is at point $x = b_1$, there is a condition of the form

$$-k_1(T)\,\frac{\partial T_1(x,t)}{\partial x}\bigg|_{x=b_1} = \frac{T_1(b_1,t) - T_2(b_1,t)}{R_{12}(T)} = -k_2(T)\,\frac{\partial T_2(x,t)}{\partial x}\bigg|_{x=b_1}, \qquad t \in (0,t^*). \tag{6}$$

Whereas in the contact space between the second and third layer, that is at point $x = b_2$, the condition has the form

$$-k_2(T)\,\frac{\partial T_2(x,t)}{\partial x}\bigg|_{x=b_2} = \frac{T_2(b_2,t) - T_3(b_2,t)}{R_{23}(T)} = -k_3(T)\,\frac{\partial T_3(x,t)}{\partial x}\bigg|_{x=b_2}, \qquad t \in (0,t^*). \tag{7}$$

The above two conditions can be often formulated with the use of contact conductance for the interface [34]:

$$h_z(T) = \frac{1}{R_z(T)}, \qquad z \in \{12,23\}.$$

The temperature distribution in the initial moment of time is known

$$T_s(x,0) = \psi_s(x), \qquad x \in [b_{s-1}, b_s]. \tag{8}$$

In the common points the consistency of the respective conditions is assumed.

The unknown element in the discussed inverse problem is the heat flux q_{at} and the necessary additional information is delivered by the measurements of temperature read in the internal point of the region

$$T_s(x_m,t_i) = U_i, \qquad i = 1,\ldots,N, \tag{9}$$

where $s \in \{1,2,3\}$ is so that $x_m \in [b_{s-1}, b_s)$, and N denotes the number of measurements.

The sought heat flux depends on parameters $q_1, q_2, \ldots, q_I$, the values of which must be determined. If in the considered problem the heat flux q_{at} is given, then it is the direct problem. Solution of the direct problem delivers the values $V_i(q)$ of temperature at point x_m corresponding to this heat flux. By using the obtained values the Tikhonov functional is constructed, which defines the error of current approximate solution

$$F(q) = \|U - V(q)\|^2 + \gamma\,\|\xi - q\|^2 = \sum_{i=0}^{N}\left(U_i - V_i(q)\right)^2 + \gamma\sum_{i=0}^{I}\left(\xi_i - q_i\right)^2, \tag{10}$$

where $q = [q_1,\ldots,q_I]^\intercal$, $V(q) = \left[V_0(q),\ldots,V_N(q)\right]^\intercal$, $U = \left[U_0,\ldots,U_N\right]^\intercal$, $\gamma > 0$ is the regularization parameter and $\xi = [\xi_1,\ldots,\xi_I]^\intercal$ is an a priori given approximation to the unknown heat flux q, and $^\intercal$ denotes the transpose. The Tikhonov functional (10) is next minimized in order to determine the desired heat flux q_{at} so that the approximate values of temperature are as close as possible to the measured values.

3. The solution procedure

The direct problem is solved with the aid of implicit scheme of the finite difference method [34–36]. This method requires the discretization of the considered region which is done by introducing the appropriate mesh. The layers are divided into n_s, $s = 1, 2, 3$, subintervals which makes the following meshes in the successive layers

$$S_1 = \{x_i : \ x_i = b_0 + i\,\Delta x_1, \ i = 0, 1, \ldots, n_1\}, \tag{11}$$

$$S_2 = \{x_i : \ x_i = b_1 + (i - n_1 - 1)\,\Delta x_2, \ i = n_1 + 1, \ldots, n_1 + n_2 + 1\}, \tag{12}$$

$$S_3 = \{x_i : \ x_i = b_2 + (i - n_1 - n_2 - 2)\,\Delta x_3, \ i = n_1 + n_2 + 2, \ldots, n_1 + n_2 + n_3 + 2\}, \tag{13}$$

where $\Delta x_1 = \frac{b_1 - b_0}{n_1}$, $\Delta x_2 = \frac{b_2 - b_1}{n_2}$, $\Delta x_3 = \frac{b_3 - b_2}{n_3}$. Because of the non-zero thermal resistances two nodes are given in the contact of the layers. The first one corresponds to the end of previous layer and the second one – to the beginning of next layer. The spatial mesh in the whole region is defined as the sum of meshes introduced in the respective layers $S_x = S_1 \cup S_2 \cup S_3$. Whereas the time interval is divided into m equal subintervals which makes the following time mesh

$$S_t = \{t_j : \ t_j = j\,\Delta t, \ j = 0, 1, \ldots, m\}, \tag{14}$$

where $\Delta t = \frac{t^*}{m}$. Finally, the mesh for the unsteady problem of heat conduction is defined as the cartesian product of the spatial and time meshes $S = S_x \times S_t$.

In the internal nodes of each layer the discretization of equation (1) is performed by means of the implicit scheme of order $O\big((\Delta x_s)^2 + \Delta t\big)$ leading to the difference equation of the form

$$-r_s \frac{\overline{k}_{s,i-1/2}}{c_{s,i}\,\varrho_{s,i}} T^{j+1}_{s,i-1} + \left(1 + r_s \frac{\overline{k}_{s,i-1/2} + \overline{k}_{s,i+1/2}}{c_{s,i}\,\varrho_{s,i}}\right) T^{j+1}_{s,i} - r_s \frac{\overline{k}_{s,i+1/2}}{c_{s,i}\,\varrho_{s,i}} T^{j+1}_{s,i+1} = T^{j}_{s,i}, \tag{15}$$

where $r_s = \frac{\Delta t}{(\Delta x_s)^2}$, $T^j_{s,i} := T_s(x_i, t_j)$, $c_{s,i} = c_s(T^j_{s,i})$, $\varrho_{s,i} = \varrho_s(T^j_{s,i})$ and $\overline{k}_{s,i+1/2} = \frac{2\,k_{s,i}\,k_{s,i+1}}{k_{s,i} + k_{s,i+1}}$ is the harmonic mean of thermal conductivity coefficient in the temperature interval $[T^j_{s,i}, T^j_{s,i+1}]$, and $\overline{k}_{s,i-1/2} = \frac{2\,k_{s,i-1}\,k_{s,i}}{k_{s,i-1} + k_{s,i}}$ is the harmonic mean of thermal conductivity coefficient in interval $[T^j_{s,i-1}, T^j_{s,i}]$ [35,36].

The boundary conditions are discretized so that the convergence order of discretization of equation (1) is maintained. For the boundary condition of the second order on the outer surface the following difference equation is obtained

$$3\,w_1\,T^{j+1}_{1,0} - 4\,w_1\,T^{j+1}_{1,1} + w_1\,T^{j+1}_{1,2} = q^{j+1/2}_{at} - \varepsilon\,\sigma\left((T^j_{1,0})^4 - T^4_\infty\right), \tag{16}$$

where $w_1 = \frac{\overline{k}_{1,0}}{2\,\Delta x_1}$ and $q^{j+1/2}_{at} := q_{at}(t_j + \Delta t/2)$.

The interface boundary condition in the contact of the first and second layer (6) is transformed into two difference equations of the form

$$-w_{1,n_1}\,T^{j+1}_{1,n_1-2} + 4\,w_{1,n_1}\,T^{j+1}_{1,n_1-1} - \left(3\,w_{1,n_1} + \overline{R}^{-1}_{12}\right) T^{j+1}_{1,n_1} + \overline{R}^{-1}_{12}\,T^{j+1}_{2,n_1+1} = 0, \tag{17}$$

$$w_{2,n_1+1}\,T^{j+1}_{2,n_1+3} - 4\,w_{2,n_1+1}\,T^{j+1}_{2,n_1+2} + \left(3\,w_{2,n_1+1} + \overline{R}^{-1}_{12}\right) T^{j+1}_{2,n_1+1} - \overline{R}^{-1}_{12}\,T^{j+1}_{1,n_1} = 0, \tag{18}$$

where $w_{s,i} = \frac{\overline{k}_{s,i}}{2\,\Delta x_s}$ and $\overline{R}_{12} = \frac{2\,R_{12}(T^j_{1,n_1})\,R_{12}(T^j_{2,n_1+1})}{R_{12}(T^j_{1,n_1}) + R_{12}(T^j_{2,n_1+1})}$.

Next, for the interface boundary condition in the contact of the second and third layer (7) the following two difference equations are received

$$-w_{2,N_2}\,T^{j+1}_{2,N_2-2} + 4\,w_{2,N_2}\,T^{j+1}_{2,N_2-1} - \left(3\,w_{2,N_2} + \overline{R}^{-1}_{23}\right) T^{j+1}_{2,N_2} + \overline{R}^{-1}_{23}\,T^{j+1}_{3,N_2+1} = 0, \tag{19}$$

$$w_{2,N_2+1}\,T^{j+1}_{3,N_2+3} - 4\,w_{3,N_2+1}\,T^{j+1}_{3,n_2+2} + \left(3\,w_{3,n_2+1} + \overline{R}^{-1}_{12}\right) T^{j+1}_{3,N_2+1} - \overline{R}^{-1}_{12}\,T^{j+1}_{2,N_2} = 0, \tag{20}$$

where $N_2 := n_1 + n_2 + 1$, $w_{s,i} = \frac{\overline{k}_{s,i}}{2\,\Delta x_s}$ and $\overline{R}_{23} = \frac{2\,R_{23}(T^j_{2,N_2})\,R_{23}(T^j_{3,N_2+1})}{R_{23}(T^j_{2,N_2}) + R_{23}(T^j_{3,N_2+1})}$.

Putting together the above equations and including the boundary condition of the first kind on the inner surface leads to the pentagonal system of linear equations of the form

$$\mathbf{A}^j\,\mathbf{T}^{j+1} = \mathbf{f}^j. \tag{21}$$

Matrix $\mathbf{A}^j$ contains the material parameters dependent on temperature, therefore it changes in each step of calculations. The obtained system is of dimensions $(n_1 + n_2 + n_3 + 2) \times (n_1 + n_2 + n_3 + 2)$.

Solution of the direct problem (1)–(9) for the given heat flux delivers the values $V(q)$ of temperature in the measurement point enabling to determine the value of Tikhonov functional F. Minimization of this functional is executed by using the Levenberg-Marquardt method in the special version designed for the Tikhonov functional [28]. In this method the special element Δq^p, correcting the current approximate solution q^p, is computed on the way of solving the system of equations

$$\left((J^p)^\intercal\,J^p + \mu^p\,E\right)\Delta q^p = (J^p)^\intercal\left(U - V(q^p)\right) + \gamma\left(\xi - q^p\right), \tag{22}$$

where J denotes the sensitivity matrix, μ is the damping parameter, E denotes the identity matrix, p means the iteration number and $\gamma > 0$ is the regularization parameter. Value of the regularization parameter is determined by applying the discrepancy principle [21,37]. In the performed calculations the damping parameter μ is assumed to be 0.001.

The termination criteria of the algorithm are defined as follows

$$F(q^{p+1}) < \eta_1,$$

$$\|q^{p+1} - q^p\| < \eta_2,$$

$$p \geqslant p_{max},$$

where p_{max} is the maximal number of iterations, η_1 and η_2 are the numeric parameters. The algorithm is terminated if any of the conditions is fulfilled. The calculations are performed for $\eta_1 = 10^{-12}$, $\eta_2 = 10^{-8}$, and $p_{max} = 60$.

More information about the method, including the proof of convergence, can be found in paper [28]. However, the computational algorithm itself is similar to the algorithm for the classical version of the Levenberg-Marquardt method [32]. The measurements of temperature $U = \left[U_0, U_1, \ldots, U_N\right]^T$, initial approximation of the sought parameters q^0, value of the regularization parameter γ and a priori estimation of the sought solution ξ are assumed to be known. It is taken $p = 0$.

1. Value of the functional $F(q^p)$ is calculated.
2. Sensitivity matrix J^p is determined.
3. On the way of solving the system of equations (22) the vector Δq^p is calculated, and next the new approximation $q^{p+1} = q^p + \Delta q^p$ is determined.
4. Value of the functional $F(q^{p+1})$ is calculated.
5. If $F(q^{p+1}) \geqslant F(q^p)$, then $\mu^p = 10\,\mu^p$ is taken and algorithm returns to 3.
6. If $F(q^{p+1}) < F(q^p)$, then q^{p+1} is accepted and $\mu^p = 0.1\,\mu^p$ is taken.
7. The procedure is stopped if any of the termination criteria is fulfilled. In opposite case the iteration number increases by one and algorithm returns to 2.

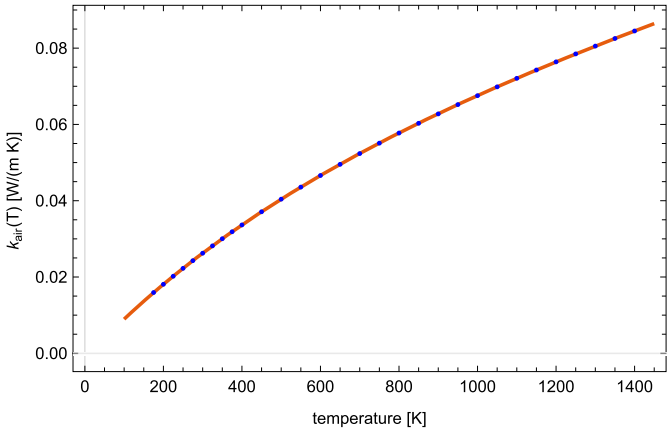

Fig. 1. Thermal conductivity coefficient of dry air dependent on temperature (dots – data taken from [38], solid line – interpolation with the third order spline).

4. Numerical calculations

The heat flux on the outer surface is reconstructed in the form of a continuous function. For this reason the absolute error (E_{abs}) and the relative error (E_{rel}) of the heat flux reconstruction are computed by using the following relations

$$E_{abs} = \frac{1}{t^*} \int_0^{t^*} |q_{ex}(t) - q_{est}(t)|\, dt, \tag{23}$$

$$E_{rel} = E_{abs} \left(\frac{1}{t^*} \int_0^{t^*} |q_{ex}(t)|\, dt \right)^{-1} 100\%, \tag{24}$$

where q_{ex} is the exact heat flux and q_{est} denotes the estimated heat flux.

The widths of the successive layers are equal to 2.2 mm, 4 mm and 114 mm, respectively. According to this, the values $b_0 = 0$ m, $b_1 = 0.0022$ m, $b_2 = 0.0062$ m and $b_3 = 0.1202$ m are taken in calculations, as well as the emissivity $\varepsilon = 0.84$ and the temperature of surrounding $T_\infty = 273$ K. Moreover, the temperature of the inner surface is assumed as $\varphi(t) = 273$ K. Temperature of the whole region in the initial moment of time is assumed to be the same and is equal to $\psi_s(x) = 273$ K, $s = 1, 2, 3$.

Thermal resistances R_{12} and R_{23} between layers can be determined with the aid of relation [36,39]:

$$R_z(T) = \frac{\delta_z}{k_z(T)}, \qquad z \in \{12, 23\}, \tag{25}$$

where δ_z denotes the width of gap between the layers and k_z expresses the thermal conductivity of the gap. It is assumed that the gap is filled with the dry air or with the appropriate glue. Values of the thermal conductivity coefficient of the dry air are taken from [38]. Next, the taken values are interpolated with the third order spline and such obtained function is used in calculations in case of material parameters dependent on temperature (see Fig. 1). In case of the constant parameters two values of the thermal conductivity coefficient of dry air are used in calculations. The value in temperature 273 K which is $k_{air} = 0.0241$ W/(m K), and the mean value $k_{air} = 0.0578$ W/(m K) in the temperature interval $[273, 1300]$ determined from relation

$$k_{air} = \left(\frac{1}{1027} \int_{273}^{1300} \left(k_{air}(T)\right)^2 dT \right)^{1/2}. \tag{26}$$

Whereas in case of glue filling the gaps, the value of its thermal conductivity coefficient is taken as $k_g = 0.032$ W/(m K). The widths of gaps between layers are equal to 0.1 mm, 0.01 mm and 0.001 mm, respectively.

Table 1
Material properties of the layers [5].

s	Material	c_s [J/(kg K)]	ϱ_s [kg/m^3]	k_s [W/(m K)]
1	Alumino-silicate	1025	2525	2.725
2	Saffil	950	50	0.0315
3	Glass-wool	1000	26	0.03256

Table 2
Temperature dependent material properties [5].

Temperature [K]	c_2 [J/(kg K)]	k_2 [W/(m K)]	k_3 [W/(m K)]
300	950	0.0363	0.04
450	950	0.0468	0.09
800	1022.2	0.1063	0.203
1000	1064.7	0.1623	0.268
1050	1075.4	0.1788	0.284
1100	1086	0.1963	0.3

The algorithm was implemented in the Wolfram language of Mathematica 13.2 package and the computations were performed with the aid of computer with processor i7-8565U, 1.80 Ghz, 2.00 GHz, equipped with 16 GB of RAM memory.

4.1. Data independent on temperature

At first the calculations were executed for the material data independent on temperature. Their values are collected in Table 1 [5].

Figs. 2–5 present the results obtained under the assumption that the gaps between layers are filled with the air. Fig. 2 shows the temperatures at the end of first and second layers for width $\delta = 0.1$ mm, different thermal resistances and air filling the gap. Differences of temperature at the end and beginning of the gaps, obtained for different widths of the gaps, are displayed in Figs. 3, 4 and 5. The difference of temperatures at the ends of gaps depends linearly on the value of thermal resistance. Ten times decrease of the thermal resistance corresponds to the ten times decrease of the temperature difference.

The next three figures present the results obtained under the assumption that the gaps are filled with the glue. The first one (Fig. 6) shows the plots of temperature at the ends of first and second layers for the gaps of width $\delta = 0.1$ mm and $\delta = 0.01$ mm. Plots of the temperature differences are displayed in two next figures: at the end and beginning of the first gap (Fig. 7) and at the end and beginning of the second gap (Fig. 8) calculated for different widths of the gaps.

4.2. Data dependent on temperature

This section includes the results of calculations executed for the following material data independent on temperature [5]: in the first layer $c_1 = 1025$ [J/(kg K)], $\varrho_1 = 2525$ [kg/m^3] and $k_1 = 2.725$ [W/(m K)], in the second layer $\varrho_2 = 50$ [kg/m^3], and in the third layer $c_3 = 1000$ [J/(kg K)] and $\varrho_3 = 26$ [kg/m^3]. Whereas the thermal conductivity coefficients of the second and third layers depend on temperature, as well as the specific heat of the second layer (Table 2). The plots of variability of these coefficients are presented in Fig. 9.

Three values of the gap widths are taken: $\delta = 0.1$ mm, $\delta = 0.01$ mm and $\delta = 0.001$ mm, as previously. The constant values of the thermal resistances, obtained for the thermal conductivity coefficient of dry air, that is $k_{air} = 0.0241$ [W/(m K)] and $k_{air} = 0.0578$ [W/(m K)], are used in calculations. The determined thermal conductivity coefficient, dependent on temperature (see Fig. 1), is also used in calculations. Plot of values of the thermal resistance between layers is presented in Fig. 10. Solid line represents the distribution in time of the thermal resistances dependent on temperature, whereas the dashed line denotes the values of constant thermal resistances. At first, the thermal resistance of the second gap (R_{23}) has a slightly higher value, but later the differences are very tiny. At the end however, a slightly higher value takes

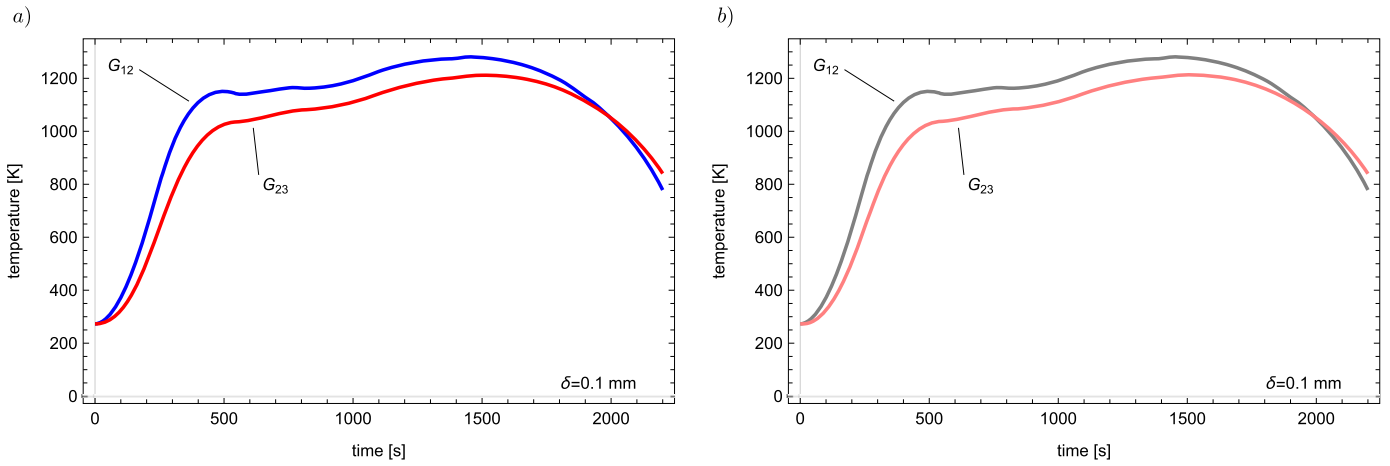

Fig. 2. Temperature at the end of first layer (G_{12}) and at the end of second layer (G_{23}) for $\delta = 0.1$ mm: *a*) for $k_{air} = 0.0241$; *b*) for $k_{air} = 0.0578$.

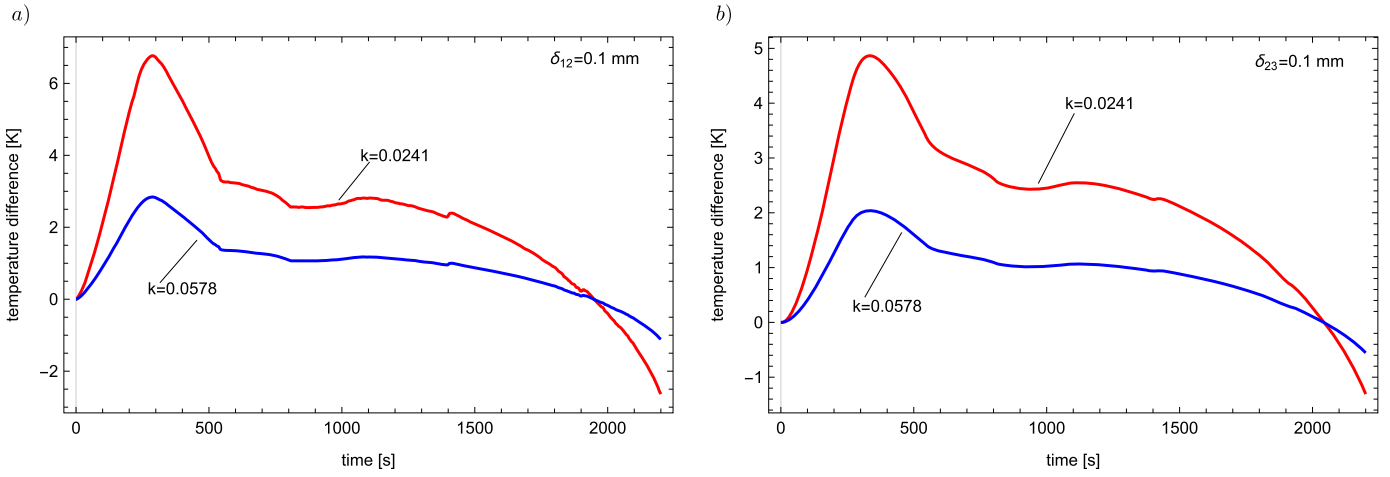

Fig. 3. Difference of temperatures at the end and beginning of gaps filled with air for $\delta = 0.1$ mm: *a*) $T_2(b_1,t) - T_1(b_1,t)$; *b*) $T_3(b_2,t) - T_2(b_2,t)$.

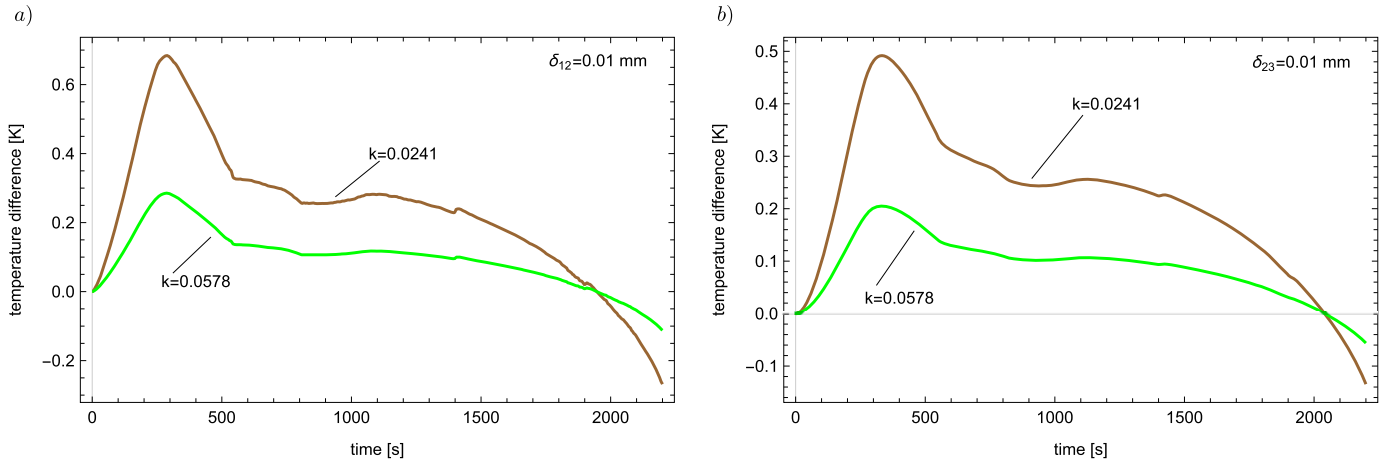

Fig. 4. Difference of temperatures at the end and beginning of gaps filled with air for $\delta = 0.01$ mm: *a*) $T_2(b_1,t) - T_1(b_1,t)$; *b*) $T_3(b_2,t) - T_2(b_2,t)$.

the thermal resistance of the first gap (R_{12}). It is connected with the distribution of the thermal conductivity coefficient of dry air (Fig. 1), used in calculations, which takes lower values in lower temperatures.

Figs. 11 and 12 show the plots of temperature differences at the end and beginning of the gaps. The temperature differences at the ends of the first gap are presented in figures *a*), whereas the temperature differences at the ends of the second gap are displayed in figures *b*). At the beginning of the process the difference of temperature is slightly bigger at the edges of the first gap, in the middle of the process the differences are similar and finally at the end of the process the bigger difference appears at the edges of the second gap. Such tendency can be observed for every value of the thermal resistance, though the bigger is the thermal resistance, the bigger are the differences between the gaps.

4.3. Inverse problem

The algorithm, described in the previous section, is applied now for reconstruction of the aerothermal heat flux q_{at} on the outer surface in

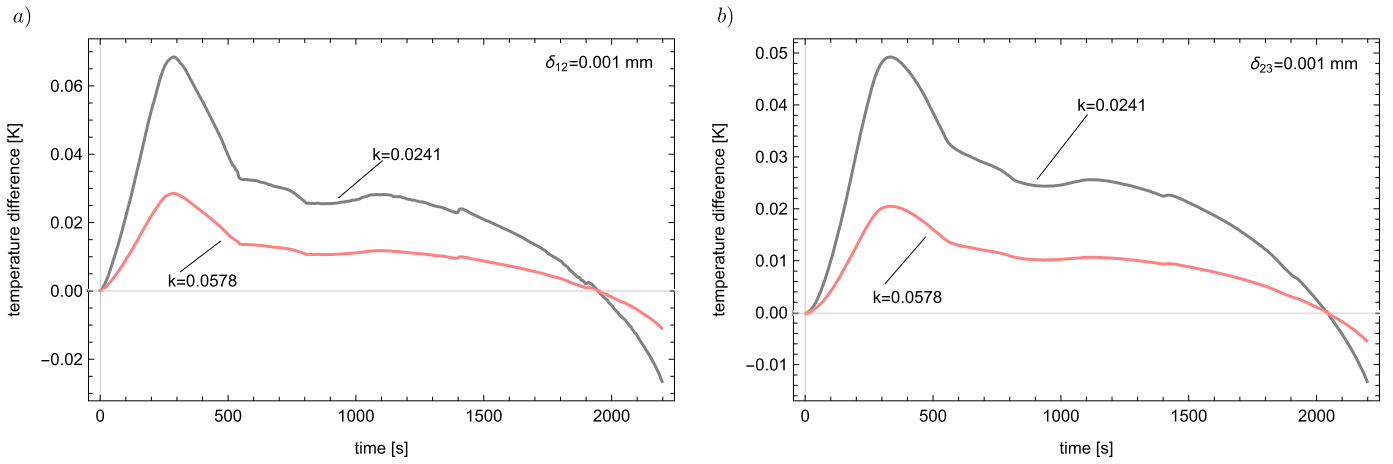

Fig. 5. Difference of temperatures at the end and beginning of gaps filled with air for $\delta = 0.001$ mm: *a*) $T_2(b_1,t) - T_1(b_1,t)$; *b*) $T_3(b_2,t) - T_2(b_2,t)$.

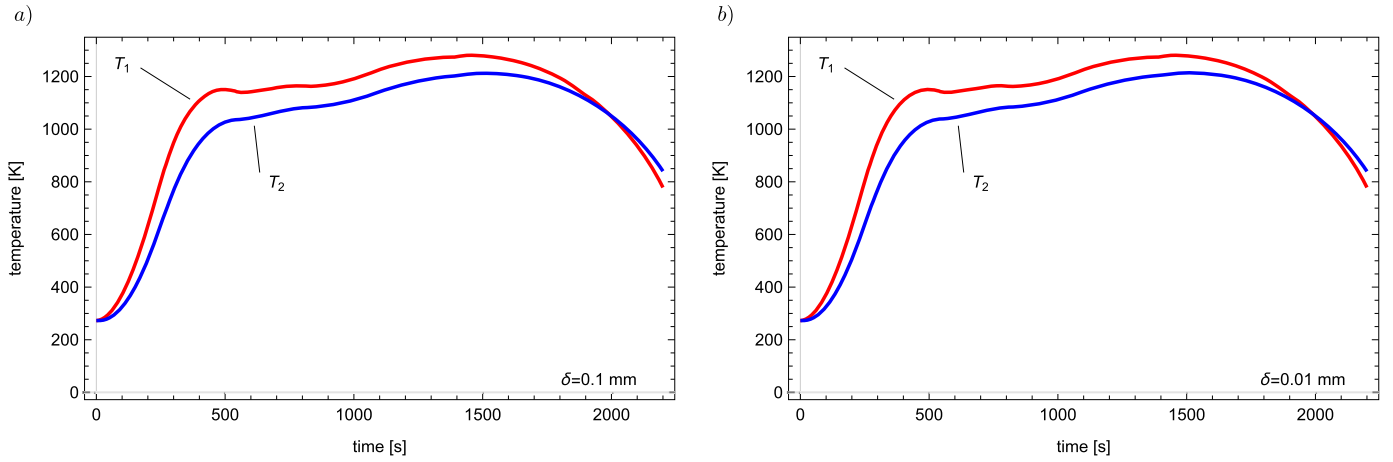

Fig. 6. Temperature at the end of first layer (T_1) and at the end of second layer (T_2) in case of gaps filled with glue: *a*) for $\delta = 0.1$ mm; *b*) for $\delta = 0.01$ mm.

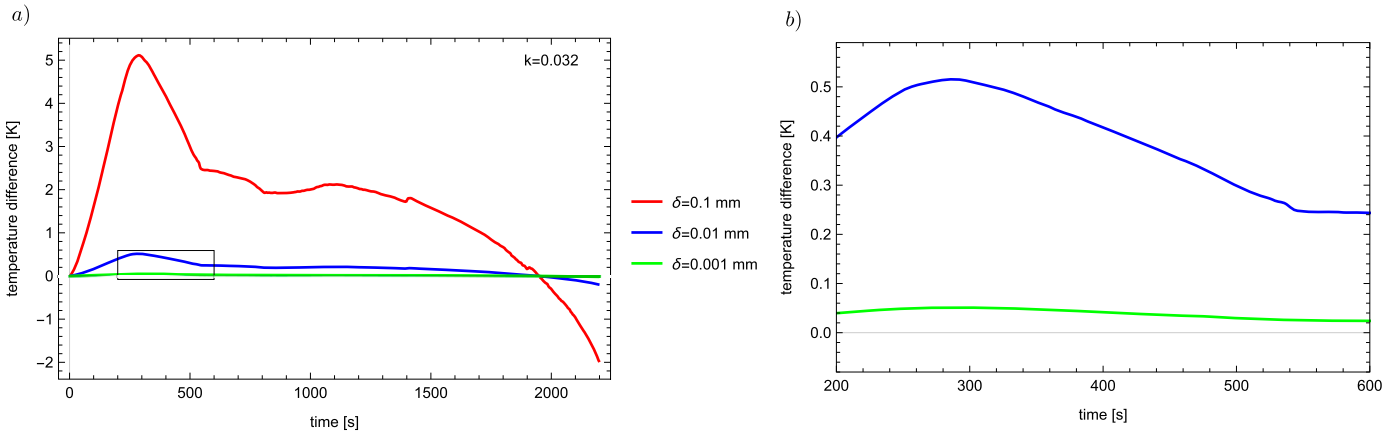

Fig. 7. *a*) Difference of temperatures at the end and beginning of the first gap filled with glue; *b*) enlargement of the part of plot *a*).

the integrated thermal protection system of a reusable launch vehicle. The atmospheric entry heating profile on the surface of such vehicle (see Fig. 13) was generated at NASA Langley Research Center [31] (see also [6,5]). The additional information, necessary for the solution of inverse problem, is given by the values of temperature in the internal point of the considered region. Location of the thermocouple is assumed at the beginning of the third layer ($x_m = b_2$). The initial data are taken from the solution of direct problem formulated for the aerothermal heat flux q_{at} presented in Fig. 13. Calculations in this direct problem were executed for the mesh $(n_1, n_2, n_3) \times m = (50, 50, 100) \times 4400$. Whereas the calculations in inverse problem were performed by using the different mesh, that is $(20, 20, 30) \times 2200$, in order to avoid the, so called, inverse crime [40]. Distribution of temperature in the measurement point, in cases of gaps filled with glue and with air and the thermal conductivity coefficient dependent on temperature, is presented in Fig. 14. The exact input data are perturbed by the random error of normal distribution and values 0.5%, 1%, 2% and 5%. Thanks to this the discussed procedure could be examined with respect to the exactness and stability of obtained results.

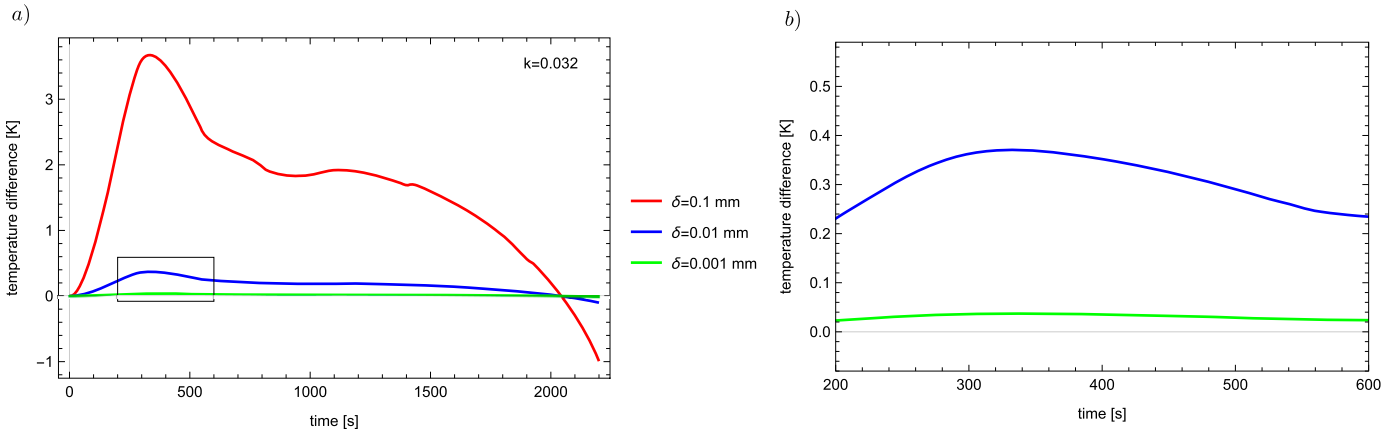

Fig. 8. *a*) Difference of temperatures at the end and beginning of the second gap filled with glue; *b*) enlargement of the part of plot *a*).

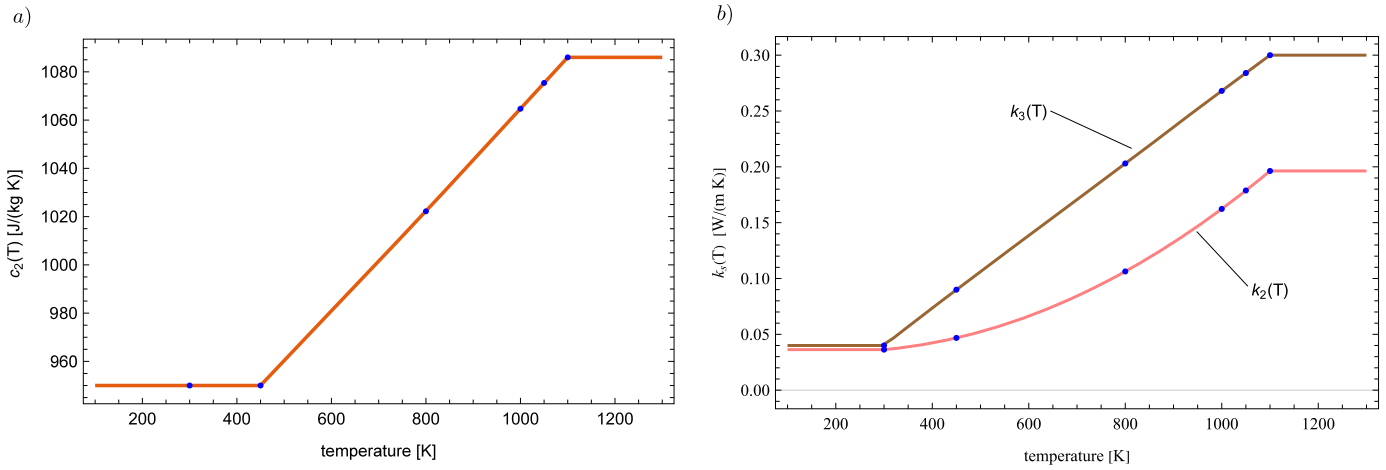

Fig. 9. Temperature dependent material properties: *a*) specific heat of the second layer; *b*) thermal conductivity coefficient of the second and third layer.

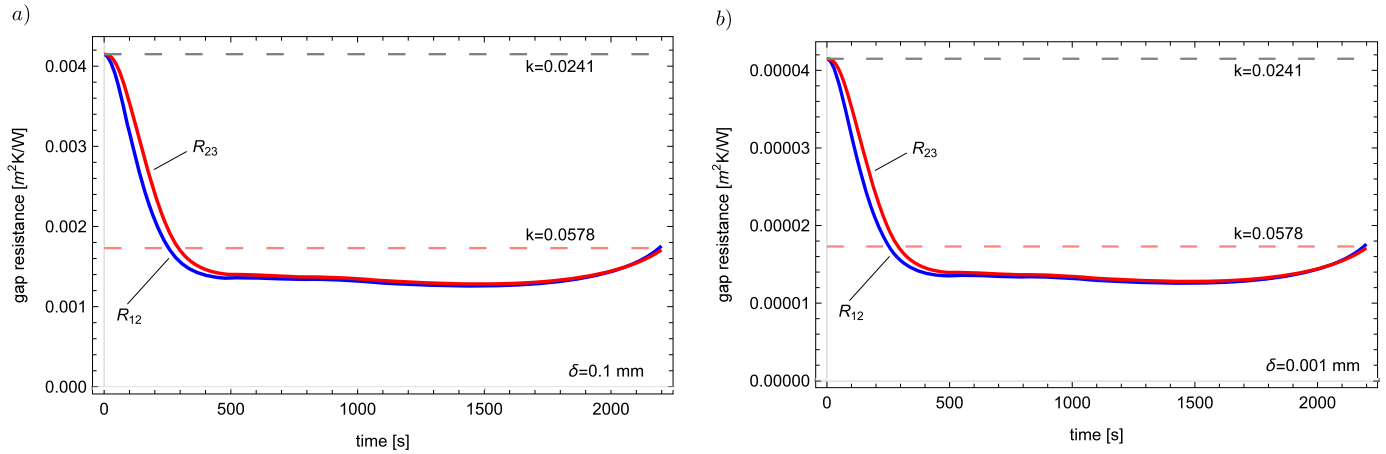

Fig. 10. Thermal resistance between the layers: *a*) for $\delta = 0.1$ mm; *b*) for $\delta = 0.001$ mm (R_{12} – thermal resistance between the first and second layers, R_{23} – thermal resistance between the second and third layers).

The heat flux is reconstructed in the form of spline of the third order constructed for the nodes $(\widehat{t}_i, q_{at,i})$, $i = 0, 1, \ldots, 20$. Additionally, it is assumed, according to the measurements [31], that in the initial moment the heat flux is equal to zero: $q_{at,0} = 0$. Thus, each time $I = 20$ values must be retrieved: $q_{at,1}$, $q_{at,2}, \ldots, q_{at,20}$. In each case the nodes are evenly distributed in the interval $(0, 2200)$, that is: $\widehat{t}_i = 110\,i$, $i = 0, 1, \ldots, 20$. The third order spline and the number of twenty nodes is chosen basing on the Authors previous experiences [32,33].

Example 1. At first the problem is solved in case of the gaps filled with air and the constant material parameters. In the presented calculations the mean value of the thermal conductivity coefficient is taken as $k_{air} = 0.0578$ W/(m K).

The errors of the heat flux reconstruction are collected in Table 3. They show that the results are very good and the reconstruction errors are always lower than the input data errors. In case of the exact input data the absolute reconstruction error is equal to 306.59 W/m^2

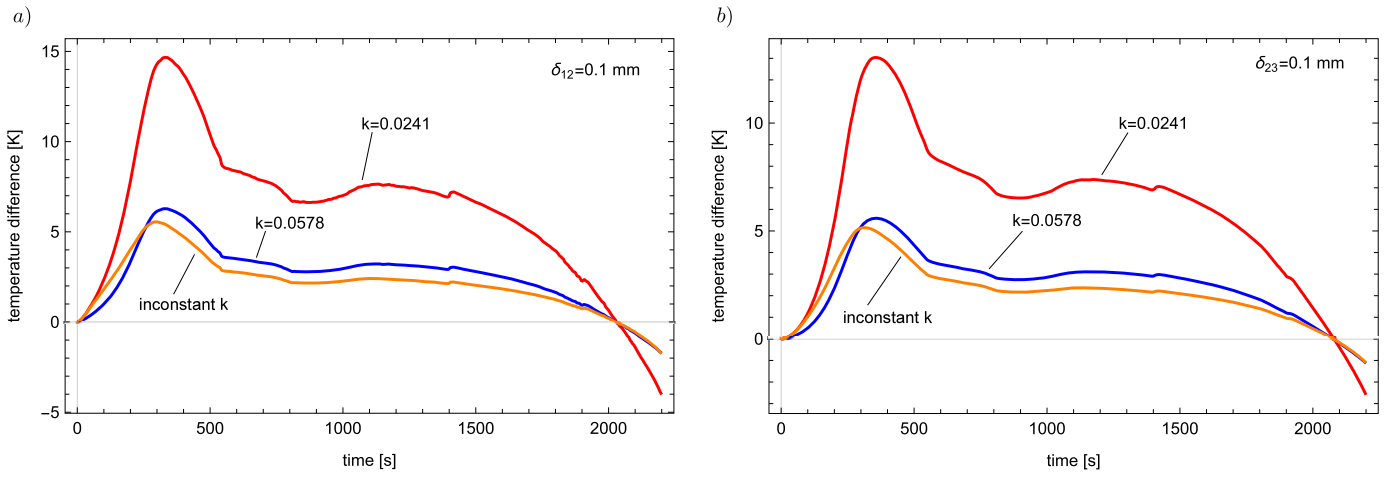

Fig. 11. Difference of temperature at the end and beginning of gaps for $\delta = 0.1$ mm: *a)* $T_2(b_1,t) - T_1(b_1,t)$; *b)* $T_3(b_2,t) - T_2(b_2,t)$.

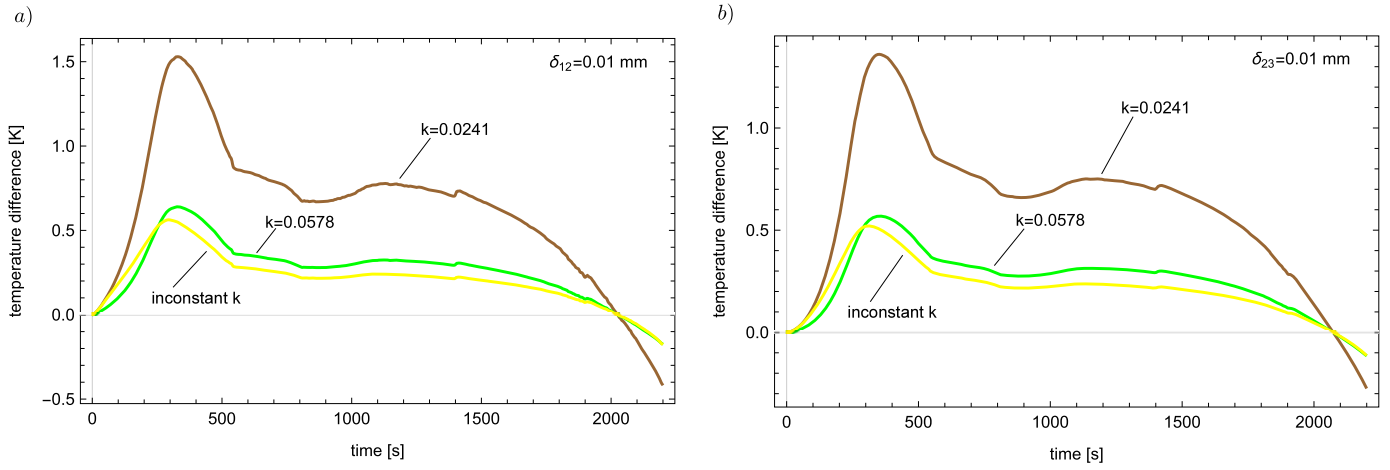

Fig. 12. Difference of temperature at the end and beginning of gaps for $\delta = 0.01$ mm: *a)* $T_2(b_1,t) - T_1(b_1,t)$; *b)* $T_3(b_2,t) - T_2(b_2,t)$.

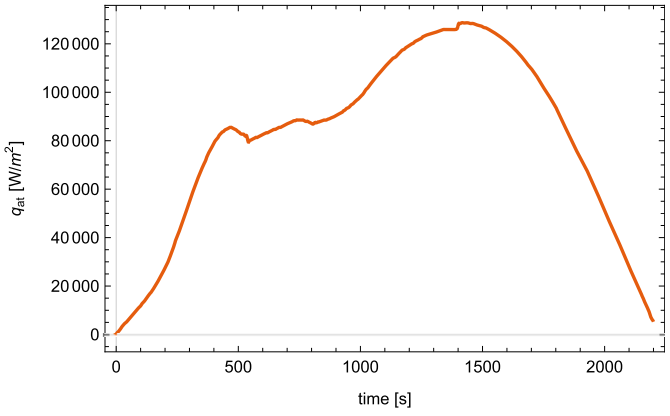

Fig. 13. Aerothermal heat flux q_{at} on the outer surface (measured by the NASA Langley Research Center [31]).

Table 3
Results of the heat flux q_{at} reconstruction for $\delta = 0.01$ mm and $k_{air} = 0.0578$ W/(m K) (Example 1).

Noise	F	E_{abs}	E_{rel} [%]
$\xi_i = 0$			
0%	569.3	306.59	0.37611
0.5%	6941.3	308.23	0.37812
1%	26922.1	322.74	0.39593
2%	107391.9	423.28	0.51927
5%	656905.8	669.46	0.82127
$\xi_i = 81515$			
0%	569.3	306.59	0.37611
0.5%	6928.0	308.23	0.37813
1%	27173.1	323.01	0.39626
2%	107639.8	423.66	0.51973
5%	656916.6	669.49	0.82130

(determined by using equation (23)), and the relative error is 0.37611% (equation (24)). These errors could be reduced by increasing the density of calculation mesh, but it would cause the extension of calculation time. The reconstruction errors increase slightly with the increase of the input data perturbations. The table presents the results for two different a priori values of the sought solution estimation (ξ). Even by having no information about the required solution and by taking the zero a priori values $\xi_i = 0$, $i = 0, \ldots, I$, the discussed method allows still to retrieve well the sought heat flux. Second part of the table includes the results obtained for the a priori value assumed as the mean value for the whole time interval, that is $\xi_i = 81515$, $i = 0, \ldots, I$. The determined minimal value of the considered functional is the most often the same or only a little bit different. In case of the burdened input data the value of the regularization parameter is changed. Thus, for example for 1% perturbation of input data the regularization parameter is equal to 10^{-10} in the first case, and 10^{-8} in the second case. The number of calculations of the objective function value reduces as well from 545 to 469. It

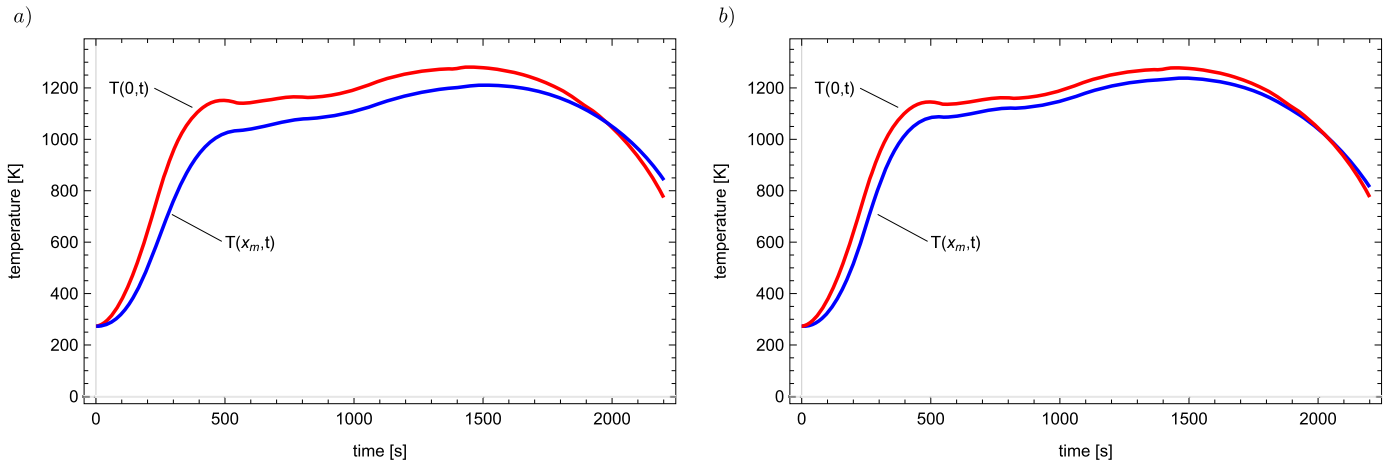

Fig. 14. Temperature on the boundary of region ($T(0,t)$) and in the measurement point ($T(x_m,t)$) for the gaps of width $\delta = 0.1$ mm filled with glue (a) and with air and the thermal conductivity coefficient dependent on temperature (b).

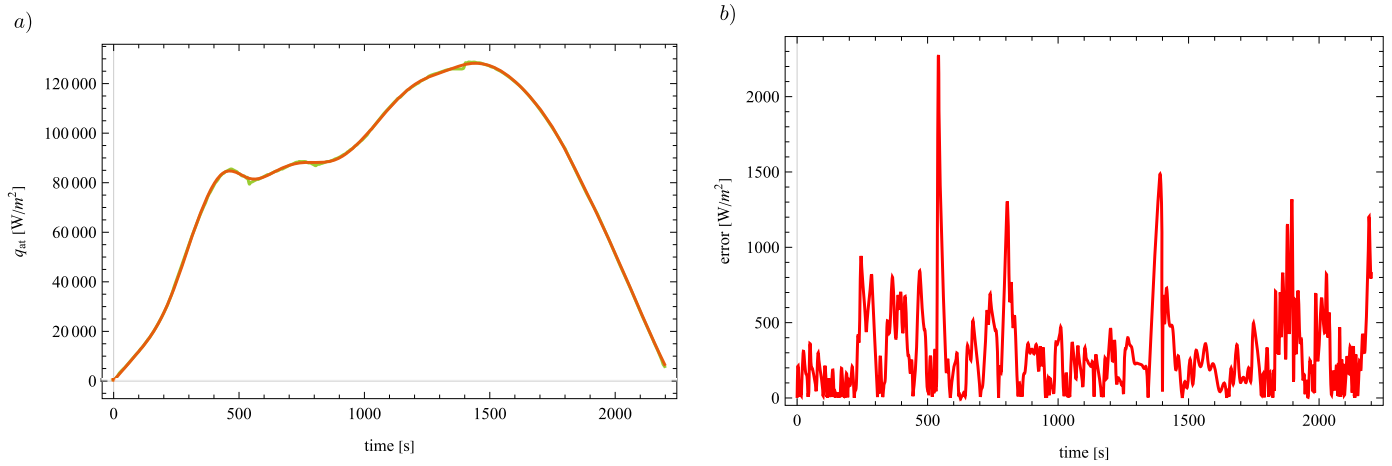

Fig. 15. Exact (green line) and reconstructed (red line) heat flux (a) together with the error of this reconstruction (b) for the exact input data ($\delta = 0.01$ mm, $k_{air} = 0.0578$ W/(m K), $\xi_i = 0$, $i = 0, 1, \ldots, I$) (Example 1). (For interpretation of the colors in the figure(s), the reader is referred to the web version of this article.)

is followed by the reduction of the full calculation time from 398 s to 346 s.

Figs. 15 *a*) and 16 *a*) present the exact value of the heat flux together with its approximation obtained from the solution of inverse problem, whereas on the right figures one can see the distribution of the absolute error of the received approximation. First set of figures show the results obtained for the exact input data and the second one – for the input data burdened by 5% error. In case of the exact input data the maximal absolute error does not exceed the value 2300 W/m^2, whereas in case of the perturbed input data (by 5% error) the maximal absolute error is lower than 2630 W/m^2. The mean errors in both discussed cases are equal to 306.59 W/m^2 and 669.49 W/m^2, respectively. In the other considered cases the distributions of absolute error, produced by the approximations of reconstructed heat flux, are very similar.

Table 4 collects the errors of temperature reconstruction in the measurement point $x_m = b_2$. For the exact input data the maximal absolute reconstruction error is equal to 1.401 K, and the mean one is 0.389 K. Considering the relative error – the maximal one does not exceed the value 0.16%, and the mean one is lower than 0.042%. The increase of the input data perturbation causes the increase of the reconstruction error, but only minor, and in each considered case the reconstruction error is much lower than the input data error. The highest values of output data errors are for the 5% input data error. In this situation the maximal absolute error is equal to 4.516 K and the value of the mean absolute error is 1.311 K. Discussing the relative error – the maximal one does not exceed 0.38%, and the mean one is lower than 0.14%. A little bit bigger maximal relative reconstruction error occurs for 2% input data error and is equal to 0.39384%. Distribution of the described errors in the whole interval is presented in Figs. 17 and 18. The results obtained in the other considered cases are very similar.

Table 4
Results of the temperature reconstruction in the measurement point for $\delta = 0.01$ mm and $k_{air} = 0.0578$ W/(m K) (Example 1).

Noise	Error [K]		Error [%]	
	max	mean	max	mean
$\xi_i = 0$				
0%	1.401	0.389	0.15621	0.04133
0.5%	1.487	0.423	0.18702	0.04598
1%	1.390	0.473	0.23059	0.05106
2%	3.306	0.658	0.39384	0.06905
5%	4.516	1.311	0.37422	0.13142
$\xi_i = 81515$				
0%	1.401	0.389	0.15621	0.04133
0.5%	1.487	0.423	0.18702	0.04598
1%	1.388	0.473	0.23069	0.05106
2%	3.340	0.658	0.39785	0.06912
5%	4.516	1.311	0.37420	0.13142

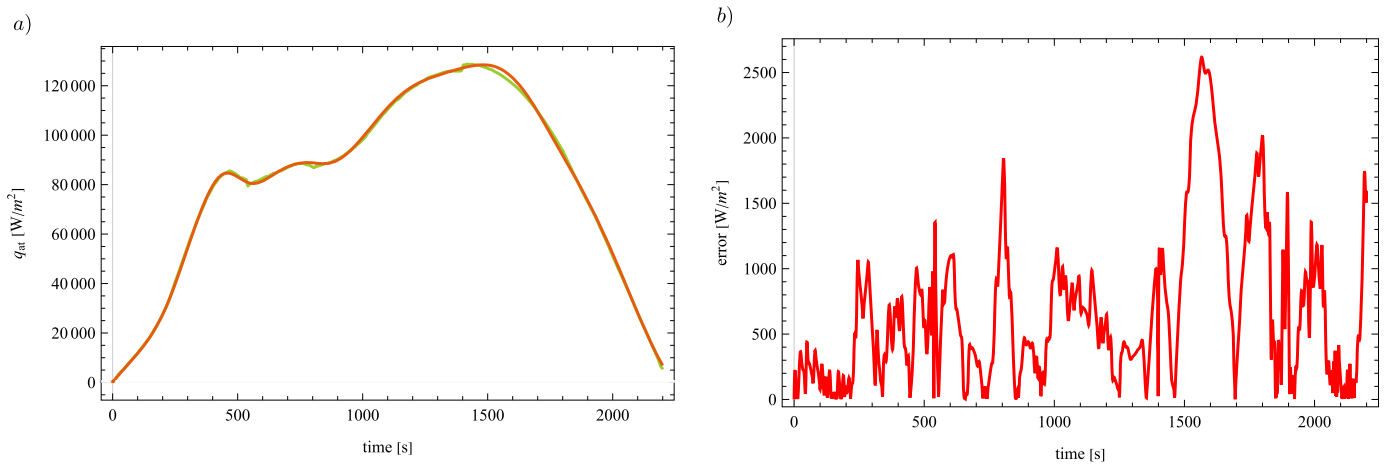

Fig. 16. Exact (green line) and reconstructed (red line) heat flux (a) together with the error of this reconstruction (b) for the input data perturbed by 5% error ($\delta = 0.01$ mm, $k_{air} = 0.0578$ W/(m K), $\xi_i = 81515$, $i = 0, 1, \ldots, I$) (Example 1).

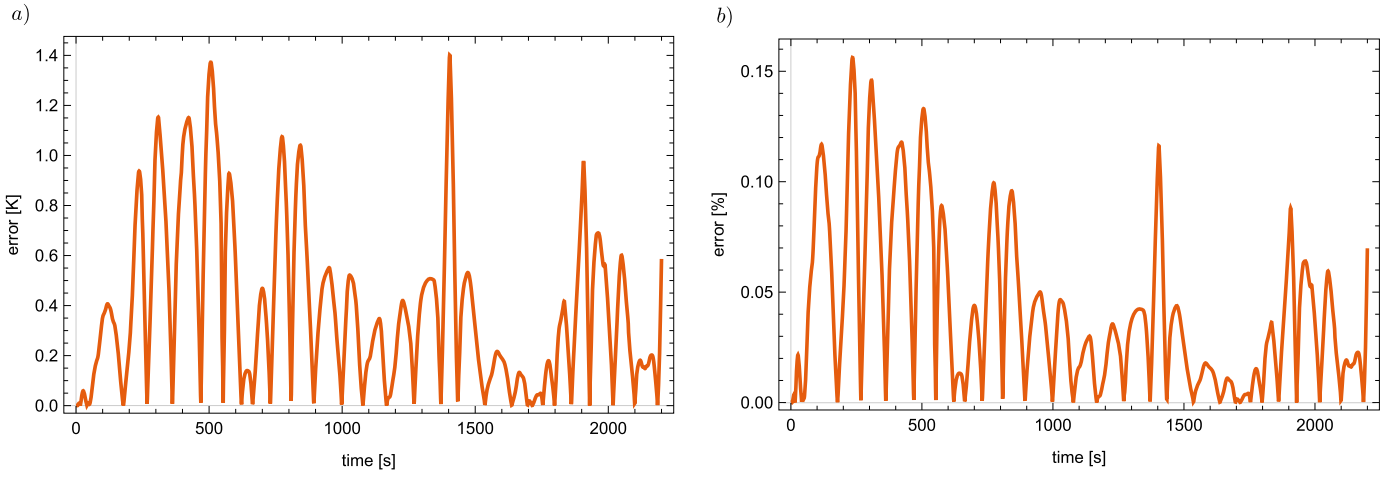

Fig. 17. Distribution of the absolute (a) and relative error (b) of temperature reconstruction in the measurement point $x_m = b_2$ for the exact input data ($\delta = 0.01$ mm, $k_{air} = 0.0578$ W/(m K), $\xi_i = 81515$, $i = 0, 1, \ldots, I$) (Example 1).

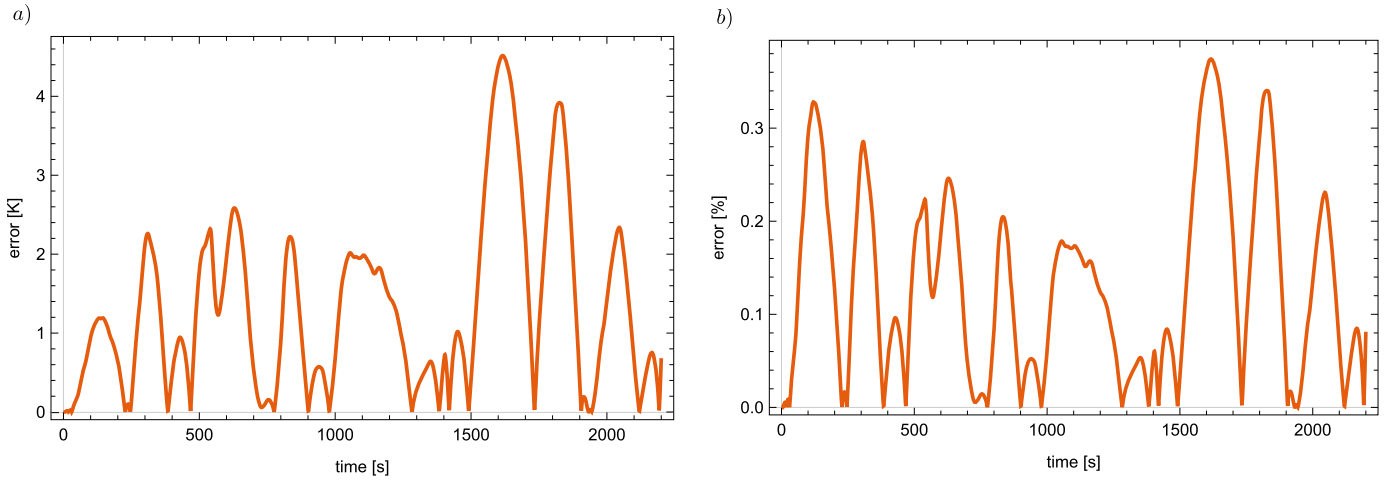

Fig. 18. Distribution of the absolute (a) and relative error (b) of temperature reconstruction in the measurement point $x_m = b_2$ for the input data perturbed by 5% error ($\delta = 0.01$ mm, $k_{air} = 0.0578$ W/(m K), $\xi_i = 0$, $i = 0, 1, \ldots, I$) (Example 1).

Fig. 19 displays the absolute errors of the heat flux restoration, obtained for the input data perturbed by error of value 2% and the gaps of width $\delta = 0.1$ mm and $\delta = 0.001$ mm. The maximal absolute errors in these cases do not exceed the values 2125 W/m^2 and 2650 W/m^2, respectively. Meanwhile, the mean values of these errors are equal to 333.96 W/m^2 and 394.93 W/m^2, respectively. Next, Fig. 20 presents the errors of temperature reconstructed in the measurement point for the gap of width $\delta = 0.1$ mm. Each time these errors are low and they are much lower in comparison with the input data errors. In case of the exact input data the maximal relative error of temperature reconstruction

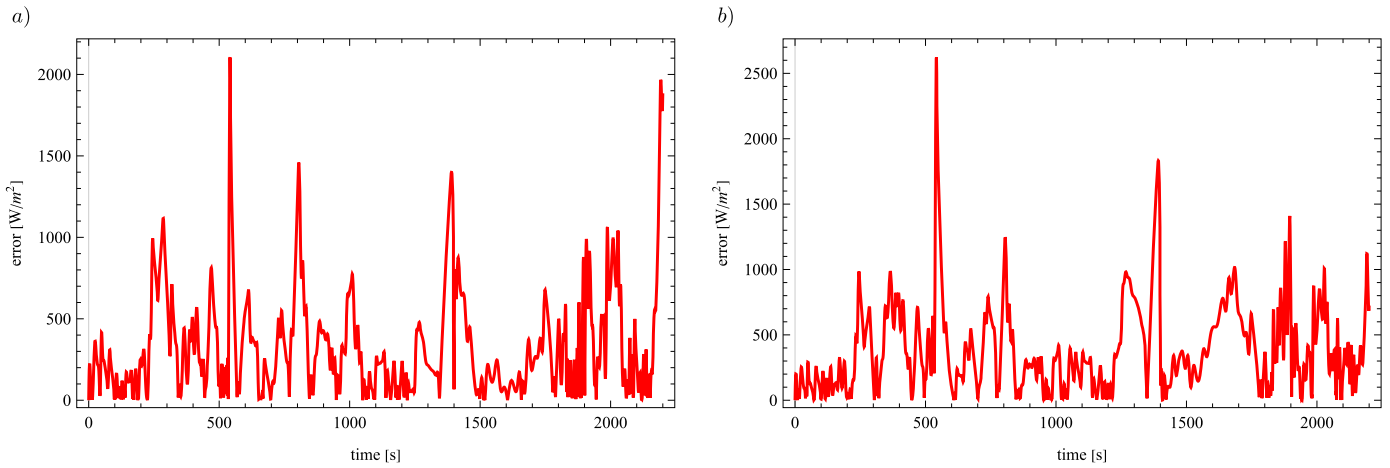

Fig. 19. Distribution of absolute error of the heat flux reconstruction for input data perturbed by 2% error ($k_{air} = 0.0578$ W/(m K), $\xi_i = 0$, $i = 0, 1, \ldots, I$): *a*) $\delta = 0.1$ mm, *b*) $\delta = 0.001$ mm (Example 1).

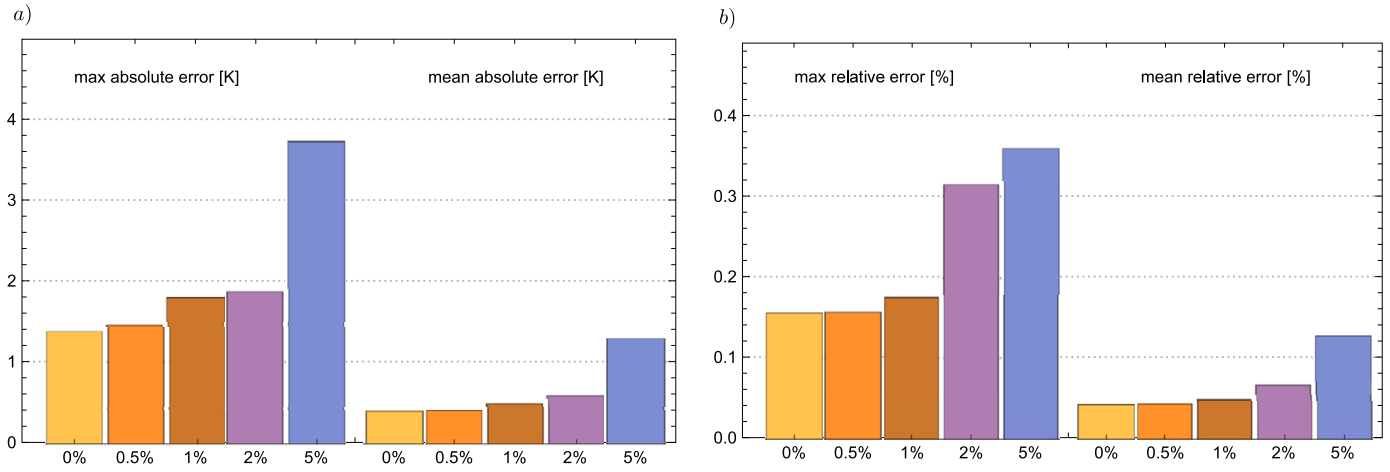

Fig. 20. Maximal and mean absolute (*a*) and relative (*b*) errors of temperature reconstruction in the measurement point ($\delta = 0.1$ mm, $k_{air} = 0.0578$ W/(m K), $\xi_i = 0$, $i = 0, 1, \ldots, I$) (Example 1).

is equal to 1.38 K, and the mean one is 0.38 K. These values influence obviously the values of relative errors – the maximal relative error is at the level of 0.16%, whereas the mean one is 0.04%. In case of the perturbed input data the reconstruction errors increase slightly with the increase of the input data perturbation. So, for the biggest perturbations the restoration errors are: the maximal absolute error – 3.73 K, the mean absolute error – 1.28 K, the maximal relative error – 0.36% and finally the mean relative error is 0.13%. In the other investigated cases the errors of temperature reconstruction have very similar values.

Table 5
Results of the heat flux q_{at} reconstruction for $\delta = 0.1$ mm, $k_g = 0.032$ W/(m K) (Example 2).

Noise	F	E_{abs}	E_{rel} [%]
0%	543.7	308.37	0.37830
0.5%	7055.6	297.37	0.36481
1%	27123.1	331.65	0.40685
2%	106843.8	404.58	0.49633
5%	642423.3	823.09	1.00974

Example 2. In the next example it is assumed that the gaps between layers are filled with glue, thermal conductivity coefficient of which is equal to $k_g = 0.032$ W/(m K). This time the calculations are executed for the a priori values $\xi_i = 0$, $i = 0, 1, \ldots, I$.

The results of the heat flux q_{at} restoration for the gaps of width $\delta = 0.1$ mm are collected in Table 5. The obtained results are very good and the reconstruction errors each time are very small. In case of the exact input data the absolute reconstruction error is equal to 308.37 W/m^2 (computed by using equation (23)), and the relative one is 0.3783% (equation (24)). The values of errors are influenced by the density of calculation mesh. Increase of the mesh density suppose to lead to decrease of the output data errors, but at the cost of increasing calculation time. Bigger input data errors entail the bigger errors of the heat flux reconstruction, but only slightly bigger. In case of input data burdened by the highest error, the absolute and relative reconstruction errors are not bigger than 823.1 W/m^2 and 1.01%, respectively.

Fig. 21 presents the distributions of absolute errors of the heat flux reconstruction obtained for the input data perturbed by errors of values 0.5% and 2%. In the first case the maximal absolute error does not exceed the value 2260 W/m^2, whereas in the second case it is not bigger than 2980 W/m^2. The highest maximal absolute reconstruction error is observed for the input data burdened by 5% error and is not bigger than 3750 W/m^2. Mean values of the discussed errors are compiled in the third column of Table 5.

Next results, presented in Fig. 22, concern the temperature restored in the measurement point. With the increasing input data perturbations the reconstruction errors increase as well, but the observed growth is only tiny, and in each considered case the reconstruction errors are smaller than the input data errors. The maximal absolute error increases

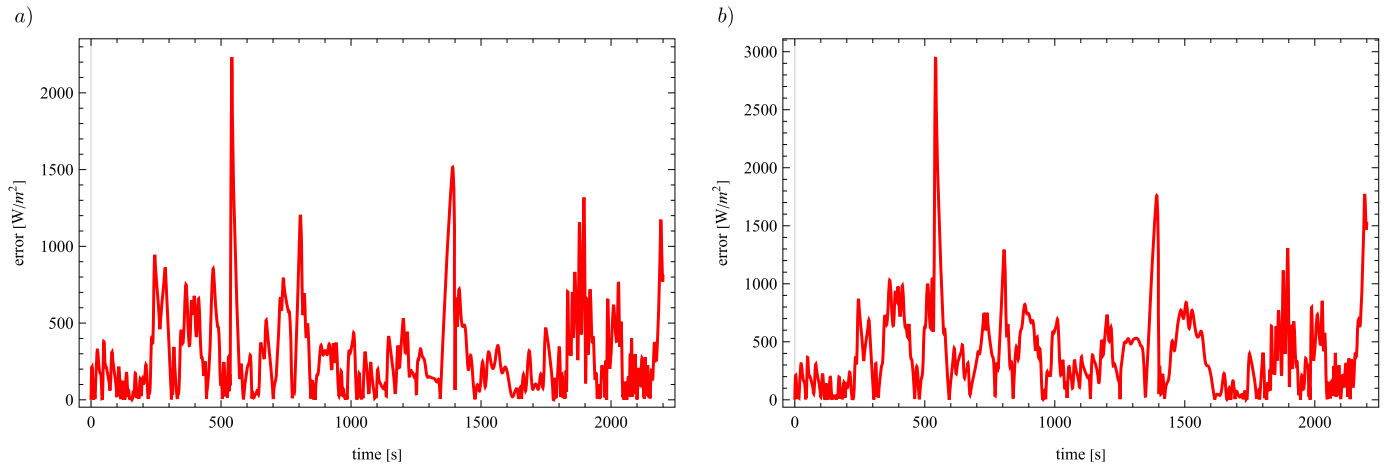

Fig. 21. Distribution of the absolute error of heat flux reconstruction for $\delta = 0.1$ mm, $k_g = 0.032$ W/(m K) and the input data perturbed by: *a*) 0.5% error, *b*) 2% error (Example 2).

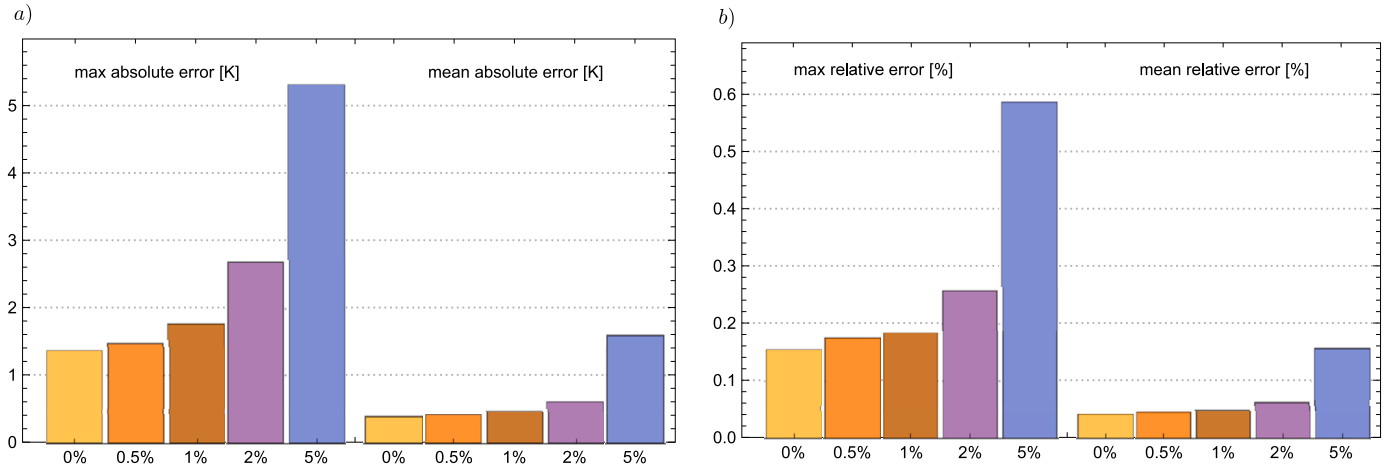

Fig. 22. Maximal and mean absolute (*a*) and relative (*b*) errors of temperature reconstruction in the measurement point ($\delta = 0.1$ mm, $k_g = 0.032$ W/(m K)) (Example 2).

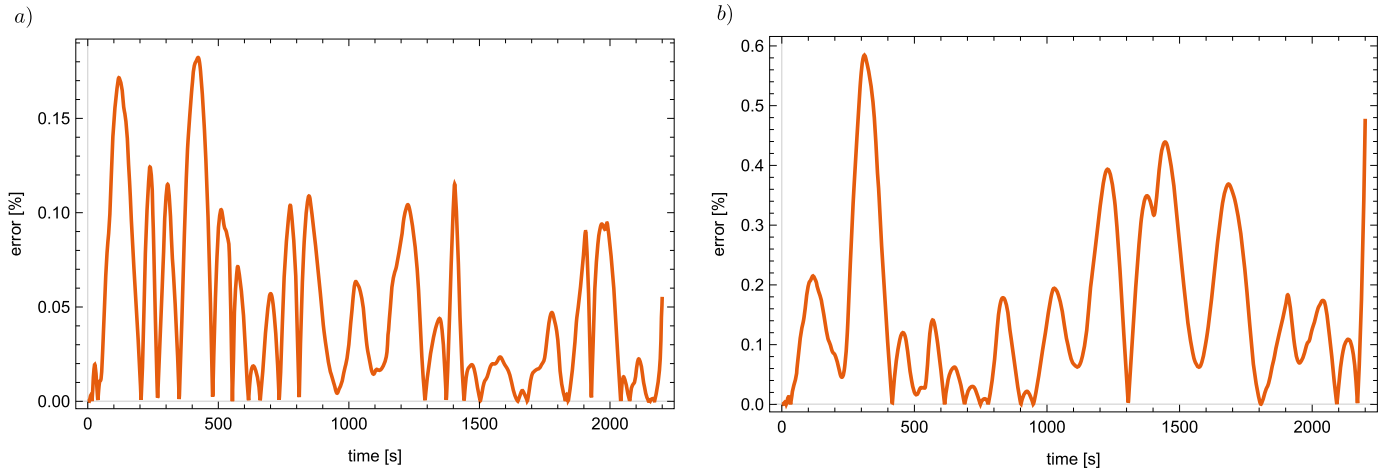

Fig. 23. Distribution of relative error of temperature reconstruction in the measurement point for $\delta = 0.1$ mm, $k_g = 0.032$ W/(m K) and the input data perturbed by: *a*) 1% error, *b*) 5% error (Example 2).

from value 1.36 K to value 5.30 K, simultaneously the mean absolute error increases from value 0.38 K to value 1.59 K. This growth corresponds to the growth of the maximal relative error from value 0.15% to value 0.58% and of the mean relative error from value 0.04% to value 0.16%. Fig. 23 shows the distribution of relative errors of temperature reconstructed in the measurement point for input data burdened by 1% and 5% errors.

Example 3. In the next step the calculations are performed for the material parameters depending on temperature (described in Subsection 4.2). The thermal conductivity coefficient is assumed as dependent on temperature as well. The results presented in this section are obtained for the gaps of width $\delta = 0.1$ mm and the zero a priori values.

Table 6 includes the results of heat flux q_{at} reconstruction. In each considered case the reconstruction errors are small. The highest values

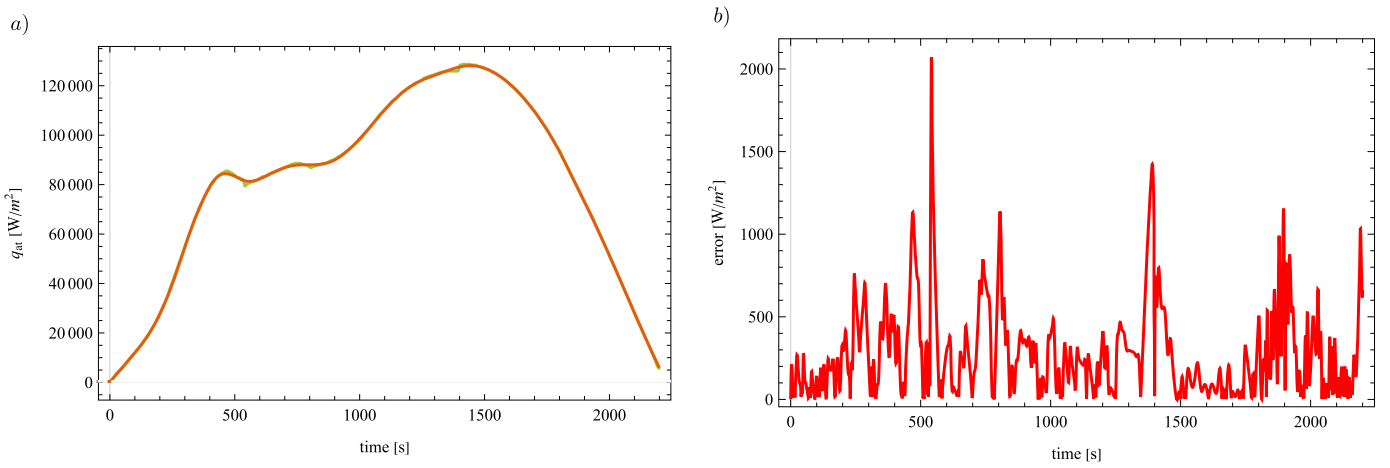

Fig. 24. Exact (green line) and reconstructed (red line) heat flux (a) together with the absolute error of this reconstruction (b) for the exact input data, $\delta = 0.1$ mm, and material parameters dependent on temperature (Example 3).

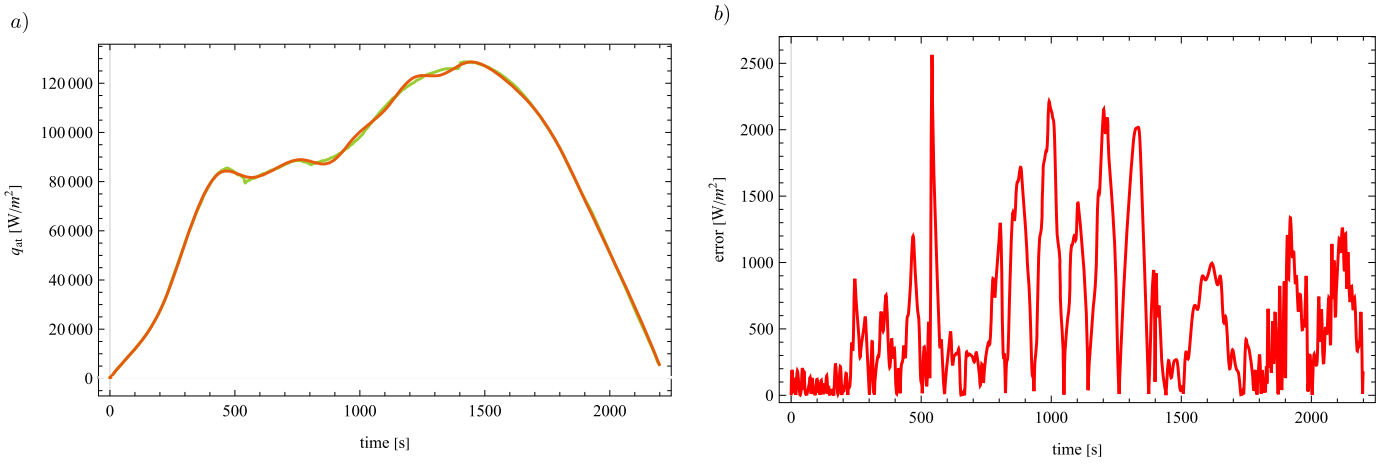

Fig. 25. Exact (green line) and reconstructed (red line) heat flux (a) together with the absolute error of this reconstruction (b) for the input data perturbed by 5% error, $\delta = 0.1$ mm, and material parameters dependent on temperature (Example 3).

Table 6
Results of the heat flux q_{at} reconstruction for material parameters dependent on temperature and $\delta = 0.1$ mm (Example 3).

Noise	F	E_{abs}	E_{rel} [%]
0%	978.6	282.05	0.34601
0.5%	7923.3	292.04	0.35827
1%	28858.2	309.69	0.37992
2%	110598.4	403.67	0.49520
5%	691738.1	613.90	0.75312

of error are observed for the input data burdened by 5% error and are equal to: absolute error – 613.90 W/m^2, relative error – 0.75312%. For lower values of the input data perturbation the output data errors are respectively lower. The value of minimized functional increases from 978.6, in case of the exact input data, to 691738.1, in case of the highest input data perturbation. The value of the regularization coefficient is equal to 10^{-10} in each case of the burdened input data.

Figs. 24 a) and 25 a) present the exact and reconstructed distribution of heat flux q_{at} (left figures) obtained for the exact input data and the input data burdened by 5% error. Figs. 24 b) and 25 b) display the respective errors of this heat flux reconstruction. In the first case the maximal absolute error does not exceed the value 2090 W/m^2, whereas in the second case it is lower than 2585 W/m^2 and this value of the output data error is the highest one observed. The mean values of the relative errors are collected in the third column of Table 6.

In the next three figures one can see the results of temperature restoration in the measurement point. Figs. 26 a) and 27 a) present the exact (solid line) and reconstructed distribution of temperature in the measurement point $x_m = b_2$ together with the temperature reconstruction (dots) calculated for the heat flux restored in the inverse problem. Meanwhile, Figs. 26 b) and 27 b) display the absolute errors of this reconstruction.

Next, Fig. 28 presents the maximal and mean errors of temperature reconstruction in the measurement point for various perturbations of input data. With increasing values of the input data error, the output data errors increase as well, but just slightly. The only exception concerns the maximal relative error obtained for the input data burdened by 1% error, which is equal to 0.2% and is lower than the error of value 0.22% obtained for the input data perturbed by lower error. However, in each considered case the restoration errors are lower than the input data perturbations. The maximal absolute error grows from value 1.97 K to value 4.6 K, whereas the mean absolute error increases from value 0.51 K to value 1.38 K. This corresponds to the growth of maximal relative error from value 0.22% to value 0.5% and the mean relative error from value 0.05% to value 0.13%.

Taking into account the depending on temperature thermophysical parameters has no influence on the exactness of results of the performed calculations. Errors of the heat flux and the temperature reconstructions are at the same level as in the previous considered examples. But it does cause the longer time of calculations. Time of solving the single direct problem increases from 0.6 s to 24.8 s, which results in an increase

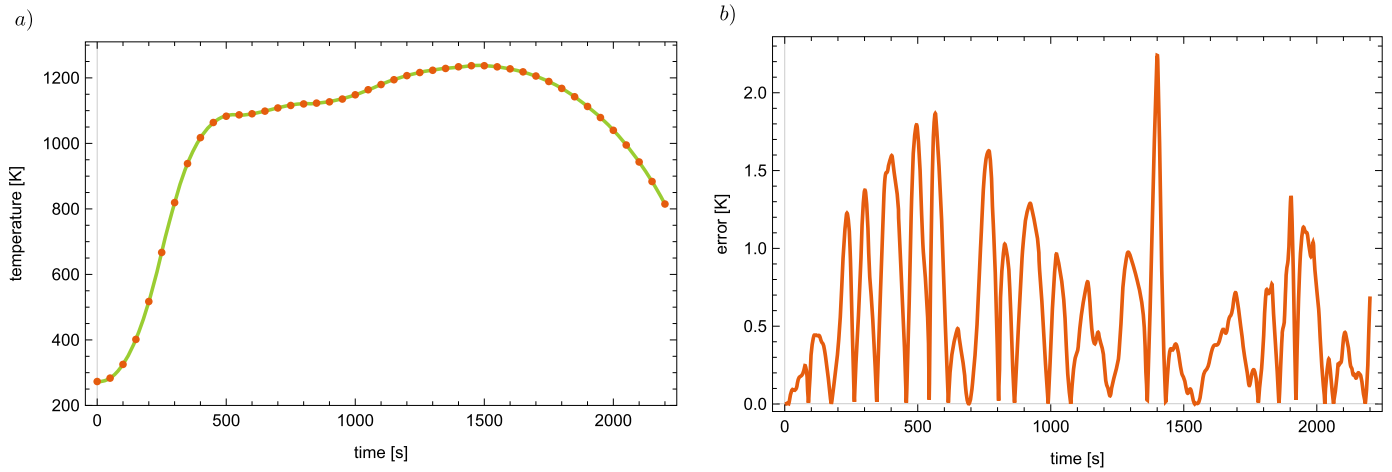

Fig. 26. Exact (solid line) and reconstructed (dots) distribution of temperature in the measurement point (a) together with the absolute error of this reconstruction (b) for the input data perturbed by 1% error, $\delta = 0.1$ mm and material parameters dependent on temperature (Example 3).

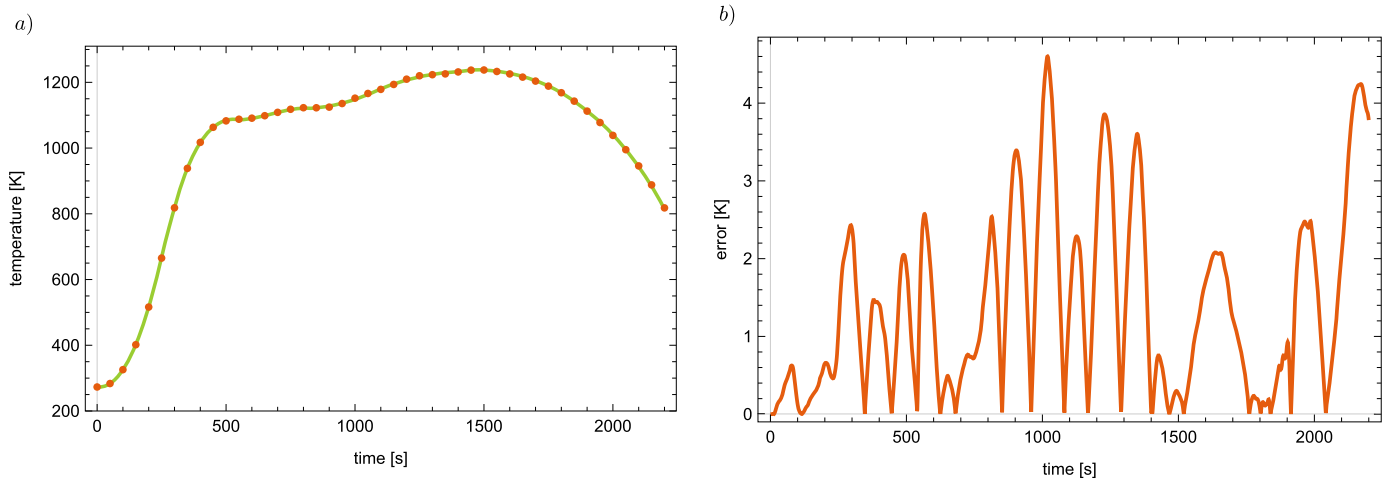

Fig. 27. Exact (solid line) and reconstructed (dots) distribution of temperature in the measurement point (a) together with the absolute error of this reconstruction (b) for the input data perturbed by 5% error, $\delta = 0.1$ mm and material parameters dependent on temperature (Example 3).

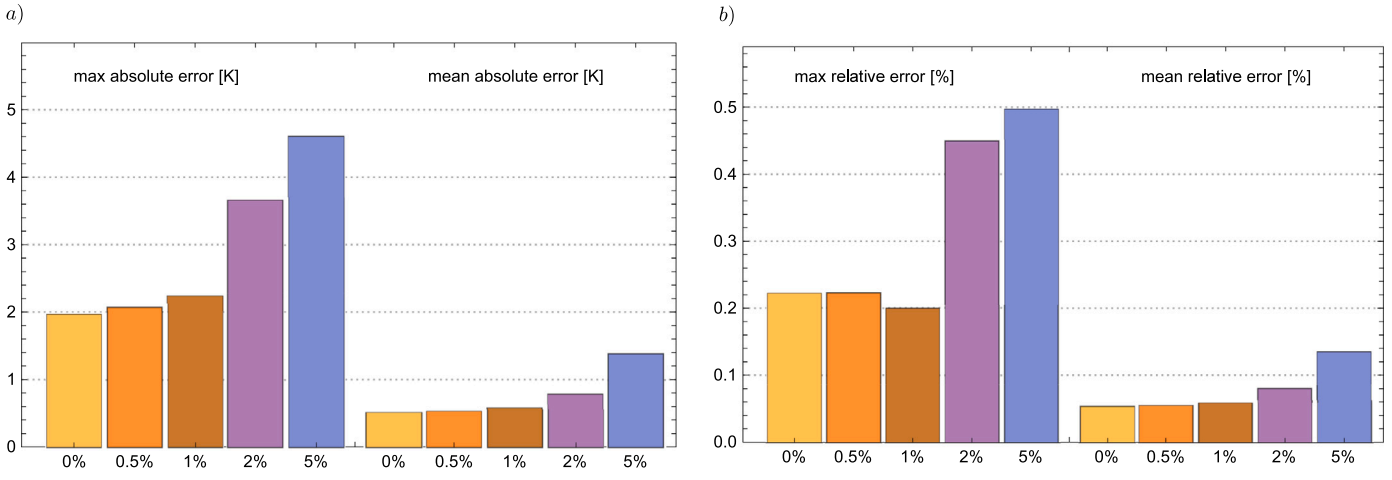

Fig. 28. Maximal and mean absolute (a) and relative (b) errors of temperature reconstruction in the measurement point for $\delta = 0.1$ mm and material parameters dependent on temperature (Example 3).

of time of the inverse problem solution. Solution of the corresponding inverse problem takes from 4800 s to 7800 s, depending on the input data perturbation and the randomly selected initial approximation. In case of the constant material parameters the time of the inverse problem solution is usually lower than 400 s.

5. Conclusions

Aim of this paper was to reconstruct the aerothermal heating of a reusable launch vehicle on the ground of the values of temperature measured in the thermal protection system of this vehicle. Using

the given temperatures and the temperatures calculated on the way of solving the appropriately formulated direct problem, the Tikhonov functional was constructed, which defined the error of approximate solution. This functional was next minimized with the aid of modified Levenberg-Marquardt method in order to reduce the difference between the measured and restored values of temperature. Whereas the corresponding direct problem was solved by applying the implicit scheme of the finite difference method. Novelty in this paper is to include in the three-layers model the thermal resistances occurring in the contact spaces between layers. Considering the parameters of material two cases were taken into account: constant parameters and parameters depending on temperature, including the thermal resistances of the contact spaces between layers also depending on temperature.

According to the previous analysis made for the case of perfect contact between layers [32], the heat flux was reconstructed in the form of third order spline for twenty interpolation points. The calculations were performed for various a priori estimations of the sought solution, various widths of the gaps and various values of the thermal conductivity coefficient of material filling the gaps. Moreover, the heat flux and the temperature were reconstructed for various errors of the input data.

All obtained results confirm the very good exactness of the proposed method and its stability with respect to the input data errors. In each considered case the heat flux is very well reconstructed. The highest restoration errors can be noticed for the highest input data perturbations (5%) and width $\delta = 0.1$ mm of the gaps filled with glue. In such worst case the mean absolute error is equal to 823.1 W/m^2 and the relative one is at the level of 1.01%. When taking for calculations the exact input data, the errors in this worst case are equal to 308.4 W/m^2 and 0.38%, respectively. The assumed density of the calculation mesh influences the values of reconstruction errors as well. By increasing the mesh density one may expect the better precision of results, that is reduction of the reconstruction errors, but it happens at the expense of longer calculation time. The restoration of temperature in the measurement point is also very good, the highest errors of temperature reconstruction do not exceed the values 7.6 K and 1.03%, respectively, whereas the mean errors in the worst case are equal to 1.6 K and 0.16%, respectively.

The plans for the future include the investigation of the two- and three-dimensional version of the considered problem, as well as the discussion on using the models with fractional derivatives for reconstructing the aerothermal heating of a reusable launch vehicle. Another plan is to reconstruct simultaneously the heat flux on the boundary of the region and the thermal resistances between the layers. To achieve this goal, the algorithm for reconstruction of the heat flux, presented in this paper, is intend to be combined with the algorithm for reconstruction of the thermal resistance in the contact of the layers, proposed by Artyukhin and Nenarokomov in work [41].

CRediT authorship contribution statement

Rafał Brociek: Conceptualization, Methodology, Writing – review & editing. **Edyta Hetmaniok:** Methodology, Writing – review & editing. **Christian Napoli:** Investigation, Visualization. **Giacomo Capizzi:** Conceptualization, Supervision. **Damian Słota:** Conceptualization, Software, Supervision, Validation, Writing – review & editing.

Declaration of competing interest

The authors declare that they have no known competing financial interests or personal relationships that could have appeared to influence the work reported in this paper.

Data availability

Data will be made available on request.

Acknowledgement

The authors express their sincere thanks to the Referees for their time and valuable remarks, which improved this paper.

References

[1] O. Uyanna, H. Najafi, Thermal protection systems for space vehicles: a review on technology development, current challenges and future prospects, Acta Astronaut. 176 (2020) 341–356.
[2] V.T. Le, N.S. Ha, N.S. Goo, Advanced sandwich structures for thermal protection systems in hypersonic vehicles: a review, Composites, Part B, Eng. 226 (2021) 109301.
[3] A.V. Gusarov, E. Poloni, V. Shklover, A. Sologubenko, J. Leuthold, S. White, J. Lawson, Radiative transfer in porous carbon-fiber materials for thermal protection systems, Int. J. Heat Mass Transf. 144 (2019) 118582.
[4] X. Wang, K. Wei, Y. Tao, X. Yang, H. Zhou, R. He, D. Fang, Thermal protection system integrating graded insulation materials and multilayer ceramic matrix composite cellular sandwich panels, Compos. Struct. 209 (2019) 523–534.
[5] O. Uyanna, H. Najafi, B. Rajendra, An inverse method for real-time estimation of aerothermal heating for thermal protection systems of space vehicles, Int. J. Heat Mass Transf. 177 (2021) 121482.
[6] S. Kumar, S.P. Mahulikar, Reconstruction of aero-thermal heating and thermal protection material response of a reusable launch vehicle using inverse method, Appl. Therm. Eng. 103 (2016) 344–355.
[7] S. Kumar, S.P. Mahulikar, Selection of materials and design of multilayer lightweight passive thermal protection system, J. Therm. Sci. Eng. Appl. 8 (2) (2016) 021003.
[8] W.-Z. Fang, Y.-Q. Tang, W.-Q. Tao, Transient thermal performance of multilayer thermal protection systems doped with phase change materials, Numer. Heat Transf., Part A, Appl. 83 (12) (2022) 1–15.
[9] A. Nenarokomov, O. Alifanov, S. Budnik, A. Netelev, Research and development of heat flux sensor for ablative thermal protection of spacecrafts, Int. J. Heat Mass Transf. 97 (2016) 990–1000.
[10] T. Nakamura, Y. Kamimura, H. Igawa, Y. Morino, Inverse analysis for transient thermal load identification and application to aerodynamic heating on atmospheric reentry capsule, Aerosp. Sci. Technol. 38 (2014) 48–55.
[11] P. Duda, A method for transient thermal load estimation and its application to identification of aerodynamic heating on atmospheric reentry capsule, Aerosp. Sci. Technol. 51 (2016) 26–33.
[12] M. Cui, Y. Zhao, B. Xu, S. Wang, X. Gao, Inverse analysis for simultaneously estimating multi-parameters of temperature-dependent thermal conductivities of an Inconel in a reusable metallic thermal protection system, Appl. Therm. Eng. 125 (2017) 480–488.
[13] O.M. Alifanov, S.A. Budnik, A.V. Nenarokomov, M.O. Salosina, Design of thermal protection based on open cell carbon foam structure optimization, Appl. Therm. Eng. 173 (2020) 115252.
[14] H.-B. Xu, K.-Y. Fan, J.-X. Yang, X.-R. Lian, F.-M. He, Z.-Y. Li, Design and evaluation of variable porosity charring composite for thermal protection system of reentry vehicles, Case Stud. Therm. Eng. 37 (2022) 102305.
[15] W. Jiang, X. Wang, R. Wang, Q. Shi, J. Zhu, Nonprobabilistic uncertain model updating and optimization design of thermal protection system, Appl. Therm. Eng. 180 (2020) 115822.
[16] X. Ren, M. Zhang, H. Nie, Optimization of multilayer thermal protection system by using phase change material under aerodynamic heating, Appl. Therm. Eng. 191 (2021) 116677.
[17] F. Wang, P. Zhang, Y. Wang, C. Sun, X. Xia, Real-time identification of severe heat loads over external interface of lightweight thermal protection system, Therm. Sci. Eng. Prog. 37 (2023) 101583.
[18] C. Ding, X. Liu, F. Xie, C. Du, Y. Wang, Heat transfer and pyrolysis gas flow characteristics of light-weight ablative thermal protection system in the blunt body, Int. J. Therm. Sci. 186 (2023) 108122.
[19] S. Wen, Y. Ma, T. Zhou, Z. Sun, Real-time estimation of thermal boundary conditions and internal temperature fields for thermal protection system of aerospace vehicle via temperature sequence, Int. Commun. Heat Mass Transf. 142 (2023) 106618.
[20] A. Tikhonov, Solution of incorrectly formulated problems and the regularization method, Sov. Math. Dokl. 4 (1963) 1035–1038.
[21] A. Tikhonov, V. Arsenin, Solution of Ill-Posed Problems, Wiley & Sons, New York, 1977.
[22] O. Alifanov, Solution of an inverse problem of heat conduction by iteration methods, J. Eng. Phys. Thermophys. 26 (1974) 471–476.
[23] O. Alifanov, S. Rumyantsev, One method of solving incorrectly stated problems, J. Eng. Phys. 34 (1978) 223–226.
[24] O. Alifanov, Inverse Heat Transfer Problems, Springer Verlag, Berlin, 1994.
[25] O. Alifanov, E. Artyukhin, S. Rumyantsev, Extreme Methods for Solving Ill-Posed Problems with Applications to Inverse Problems, Begell House, New York, 1995.
[26] O. Alifanov, Inverse problems in identification and modeling of thermal processes: Russian contributions, Int. J. Numer. Methods Heat Fluid Flow 27 (2017) 711–728.
[27] V. Vasin, G. Perestoronina, The Levenberg-Marquardt method and its modified versions for solving nonlinear equations with application to the inverse gravimetry problem, Proc. Steklov Inst. Math. 280 (2013) S174–S182.

[28] V. Vasin, The Levenberg-Marquardt method for approximation of solutions of irregular operator equations, Autom. Remote Control 73 (2012) 440–449.
[29] M. Cui, K. Yang, X. Xu, S. Wang, X. Gao, A modified Levenberg-Marquardt algorithm for simultaneous estimation of multi-parameters of boundary heat flux by solving transient nonlinear inverse heat conduction problems, Int. J. Heat Mass Transf. 97 (2016) 908–916.
[30] R. Sajedi, J. Faraji, F. Kowsary, A new damping strategy of Levenberg-Marquardt algorithm with a fuzzy method for inverse heat transfer problem parameter estimation, Int. Commun. Heat Mass Transf. 126 (2021) 105433.
[31] D. Myers, C. Martin, M. Blosser, Parametric weight comparison of current and proposed thermal protection system (TPS) concepts, in: Proc. 33rd Thermophysics Conference, AIAA, Norfolk, 1999, AIAA-99-3459.
[32] R. Brociek, E. Hetmaniok, D. Słota, Reconstruction of aerothermal heating for the thermal protection system of a reusable launch vehicle, Appl. Therm. Eng. 219 (2023) 119405.
[33] R. Brociek, E. Hetmaniok, C. Napoli, G. Capizzi, D. Słota, Estimation of aerothermal heating for a thermal protection system with temperature dependent material properties, Int. J. Therm. Sci. 188 (2023) 108229.
[34] M. Özişik, Heat Conduction, Wiley & Sons, New York, 1980.
[35] Y. Jaluria, K. Torrance, Computational Heat Transfer, Taylor & Francis, New York, 2003.
[36] B. Mochnacki, J. Suchy, Numerical Methods in Computations of Foundry Processes, PFTA, Cracow, 1995.
[37] K. Kurpisz, A.J. Nowak, Inverse Thermal Problems, Computational Mech. Publ., Southampton, 1995.
[38] Engineering ToolBox, Tech. rep., Available at: https://www.engineeringtoolbox.com, 2021. (Accessed 8 December 2022).
[39] J. Chen, X. Xu, J. Zhou, B. Li, Interfacial thermal resistance: past, present, and future, Rev. Mod. Phys. 94 (2022) 025002.
[40] J. Kaipio, E. Somersalo, Statistical and Computational Inverse Problems, Springer, New York, 2005.
[41] E. Artyukhin, A. Nenarokomov, Deriving the thermal contact resistance from the solution of the inverse heat-conduction problem, J. Eng. Phys. 46 (4) (1984) 495–499.